NACA TN 4288
10630

TECH LIBRARY KAFB, NM
0067236

NATIONAL ADVISORY COMMITTEE FOR AERONAUTICS

TECHNICAL NOTE 4288

TURBULENCE AND TEMPERATURE FLUCTUATIONS BEHIND A HEATED GRID

By R. R. Mills, Jr., A. L. Kistler, V. O'Brien, and S. Corrsin

The John Hopkins University
Baltimore, Maryland

Washington
August 1958

AFL 2811

TECH LIBRARY KAFB, NM
0067236

NATIONAL ADVISORY COMMITTEE FOR AERONAUTICS

TECHNICAL NOTE 4288

TURBULENCE AND TEMPERATURE FLUCTUATIONS BEHIND A HEATED GRID

By R. R. Mills, Jr., A. L. Kistler, V. O'Brien, and S. Corrsin

4934

CP-1

SUMMARY

In the approximately isotropic velocity and temperature fluctuation fields behind a hot grid, measurements were made of fluctuation levels and of various double and triple correlation functions.

The double and triple correlation coefficient functions are of roughly the same spatial extent for the vector and scalar fields. As anticipated from theoretical considerations, the temperature fluctuations die out more slowly than does the turbulence.

INTRODUCTION

The simplest turbulent flow is that for which the statistical properties of the field are invariant to rotation or reflection of the Cartesian coordinate system. This notion, isotropic turbulence, was introduced by Taylor in 1935 (ref. 1) and has been fruitful in permitting relatively detailed analytical studies (ref. 2).

An approximation to isotropic turbulence turns up in the high Reynolds number flow far behind a plane "porous" obstacle spanning a uniform mean flow in a duct. The customary obstacle is a square mesh biplane grid of round rods.

Although the turbulence found in natural and technological flows is ordinarily far from isotropic, many features of diverse turbulent flows, especially the spatially local features, seem to be moderately universal (ref. 3).

A comparison between the correlation equations for concomitant (incompressible) isotropic velocity and temperature fields shows differences attributable to the fact that velocity is a vector, while temperature is a scalar (refs. 4 to 6). (As pointed out in refs. 4 and 5, the work applies equally well to isotropic turbulent mixing between two different constituents, provided the molecular mass transfer coefficient is nearly constant over the concentration range encountered.) The relative

decay rates were estimated under strong simplifying assumptions, and the relative "microscales" were deduced in terms of the Prandtl number of the fluid. Since these theoretical predictions are essentially conjecture, it is necessary to determine some facts through measurement.

A comparison of the corresponding statistical properties of these two fields has not only intrinsic interest; it may also contribute eventually to an understanding of the difference between momentum and heat transport rates in turbulent shear flows with mean temperature gradients.

A "hot grid" with thermal mesh equal to momentum mesh was selected with the expectation that approximate equality of integral scales would be obtained. The analysis of reference 4 suggests that the flow with equal integral scales for velocity and temperature fields may not be the simplest case analytically but is relatively simple for experimental realization.

This work conducted at The Johns Hopkins University has been sponsored and supported financially by the National Advisory Committee for Aeronautics. Acknowledgment is made to Dr. L. S. G. Kovasznay, Mr. L. T. Miller, and Mr. J. L. Lumley for their advice and Mr. S. Bhaduri for preparing the figures.

4934

SYMBOLS

c_p specific heat at constant pressure

$E_\theta(\kappa_x)$ one-dimensional power spectrum of θ-fluctuations

$E_u(\kappa_x)$ one-dimensional power spectrum of u-fluctuations

e, e_1, e_2 output voltage of hot wire due to turbulent fluctuations; subscripts 1 and 2 distinguish between different wires

$f(r)$ longitudinal double velocity correlation coefficient, $\dfrac{\overline{u(x,y,z)u(x+r,y,z)}}{u'(x)\,u'(x+r)} = \dfrac{\overline{u_1 u_2}}{u_1' u_2'}$

$g(r)$ lateral double velocity correlation coefficient, $\dfrac{\overline{u(x,y,z)u(x,y+r,z)}}{u'^2(x)}$

i wire current

i_c output of cubing circuit, microamps

4934

CP-1 back

i_s output of squaring circuit, microamps

K thermal conductivity coefficient

$k(r)$ longitudinal triple velocity correlation, $\dfrac{\overline{u^2(x,y,z)u(x+r,y,z)}}{\left[u'(x)\right]^2 u'(x+r)} = \dfrac{\overline{u_1^2 u_2}}{u'^2 u_2'}$

L_f, L_θ integral scales of f and m, respectively

M grid mesh size for momentum and heat, M = 1 in.

$m(r)$ temperature correlation coefficient, $\dfrac{\overline{\theta(x,y,z)\,\theta(x+r,y,z)}}{\theta'(x)\;\theta'(x+r)} = \dfrac{\overline{\theta_1\theta_2}}{\theta_1'\theta_2'}$

$n(r)$ triple temperature correlation, $\dfrac{\overline{\theta^2(x,y,z)\,\theta(x+r,y,z)}}{\left[\theta'(x)\right]^2\,\theta'(x+r)} = \dfrac{\overline{\theta_1^2\theta_2}}{\theta_1'^2\theta_2'}$

Pe Peclet number, $u'\lambda_\theta/\gamma$

Pr Prandtl number, ν/γ

$p(r)$ temperature-velocity triple correlation, $\dfrac{\overline{u(x,y,z)\,\theta(x,y,z)\,\theta(x+r,y,z)}}{u'(x)\;\theta'(x)\;\theta'(x+r)} = \dfrac{\overline{u_1\theta_1\theta_2}}{u_1'\theta_1'\theta_2'}$

Re Reynolds number, $\lambda_g u'/\nu$

r space interval

S_e skewness of voltage, $\overline{e^3}/(\overline{e^2})^{3/2}$

$S_{\dot{e}}$ skewness of voltage derivative, $\overline{\left(\dfrac{\partial e}{\partial t}\right)^3}\Bigg/\left[\overline{\left(\dfrac{\partial e}{\partial t}\right)^2}\right]^{3/2}$

$S_{\Delta e}$ skewness of voltage difference, $\overline{(e_1 - e_2)^3}\Big/\left[\overline{(e_1 - e_2)^3}\right]^{3/2}$

S_u skewness of velocity, $\overline{u^3}/(\overline{u^2})^{3/2}$

$S_{\dot{u}}$ skewness of velocity derivative, $\overline{(\partial u/\partial x)^3}\Big/\left[\overline{(\partial u/\partial x)^2}\right]^{3/2}$

$S_{\Delta u}(r)$ skewness of velocity difference, $\overline{(u_1 - u_2)^3}\Big/\left[\overline{(u_1 - u_2)^2}\right]^{3/2}$

S_θ skewness of temperature fluctuation, $\overline{\theta^3}/(\overline{\theta^2})^{3/2}$

T	mean fluid temperature
t	time
$\overline{U}$	mean flow velocity
u,v	turbulent velocity fluctuations in x- and y-directions, respectively
u_1	$u(x)$
u_2	$u(x+r)$
v_1,v_2	$v_1 = v(y)$, $v_2 = v(y+r)$
x,y,z	Cartesian space coordinates, x alined with mean flow
γ	thermal diffusivity coefficient, $K/\rho c_p$
η,η_θ	length parameters in universal equilibrium theory for velocity and temperature, respectively (η is the "Kolmogoroff microscale")
θ	temperature fluctuation
θ_1,θ_2	$\theta_1 = \theta(x)$, $\theta_2 = \theta(x+r)$
κ_c,κ_0	wave numbers at lower and upper bounds of inertial subrange, respectively, corresponding to velocity spectrum except when subscript θ is used
κ_x	wave number in x-direction
$\lambda_g,\lambda_f,\lambda_\theta$	dissipation scales and lateral and longitudinal velocity and temperature fluctuations, respectively
μ	viscosity coefficient
ν	kinematic viscosity coefficient, μ/ρ
ξ	space interval in x-direction, $\equiv \Delta x$
ρ	density

Subscripts:

max	maximum
θ	wave number corresponding to temperature spectrum

Superscript:

indicates root-mean-square values, e.g., $u' = \sqrt{\overline{u^2}}$

EXPERIMENTAL EQUIPMENT

Approximately isotropic turbulence was produced at some distance behind a biplane square mesh grid of 1/4-inch-round metal rods spaced 1 inch at the centers. The grid was positioned in the wind tunnel as shown in figure 1. The signals generated by the hot-wires in the wind tunnel were fed into the circuit outlined in figure 2. In order to measure the various skewness factors and triple correlation functions presented later in this report, it was necessary to incorporate the power and operational amplifier circuit (fig. 3) to boost the signal levels to the proper input level of the squaring and cubing circuits shown in figures 4 and 5. (The auxiliary squaring and cubing circuit was developed by Mr. L. T. Miller of the Aeronautics Department, The Johns Hopkins University.)

A typical set of calibration curves for this auxiliary squaring and cubing circuit is shown in figure 6. The response of the auxiliary amplifiers was flat to approximately 10 kilocycles when used as ordinary power boosters; and when used as differentiating operational amplifiers, the response was linear with frequency to approximately 6 kilocycles (fig. 7).

The wind tunnel walls were adjusted to provide uniform mean flow over approximately 90 percent of the cross section. This configuration produces a turbulence which is not quite isotropic: $v' \approx 0.9\ u'$ at $x/M = 100$. (This is consistent with all previous measurements in which the authors have participated (see, e.g., ref. 7).

The grid was heated with 220-volt, 3-phase alternating current in order to generate approximately isotropic temperature fluctuations in this flow field. No 120-cycle-per-second periodic temperature component was detectable with this arrangement. To produce a uniform mean temperature field downstream of the grid, it was necessary to have local control over the heating current supplied to grid rods. Adjustable resistors were added to the grid heating current supply lines to achieve the desired mean temperature distribution (fig. 8).

The present arrangements generated satisfactorily homogeneous turbulence and temperature fields (fig. 9).

Turbulence and temperature root-mean-square fluctuation measurements were made with the hot-wire anemometry equipment described in reference 8. The experimental procedures for simultaneous velocity and temperature fluctuations are given in reference 9.

All the measurements were made at a mean speed of 14 feet per second and a mean temperature rise (across the grid) of about 5° C. The resulting temperature fluctuations were inconveniently small, but this ensured negligible influence of density variations upon the fully developed turbulent velocity field, as attested by both turbulence level and velocity correlation measurements.

Because of the extremely small temperature fluctuations, it was necessary to use unusually high resistance hot-wires, 0.00005-inch platinum of about 75- to 150-ohm resistance and about 0.1 inch long. No length corrections were applied to the data. The high resistance necessitated correction for heating current fluctuations when the system was operated as an anemometer. The uncompensated time constant of these wires was about 0.1 millisecond. In this particular flow field, the wire current giving equal root-mean-square signal contributions from velocity and from the temperature fluctuations was 5.5 milliamperes. The sensitivity to temperature was approximately linear with current, and the sensitivity to velocity was proportional to the current cubed for currents less than roughly 0.7 milliampere.

EXPERIMENTAL PROCEDURE

The decays of the temperature and velocity fluctuations were measured with a single hot-wire used at various operating conditions so that the separate decay functions could be calculated (ref. 9). The correlation was zero with the accuracy of the data.

Two-point double correlations were measured with two wires mounted on a traversing device that located the wires with respect to each other within 0.005 inch. One wire was held stationary and the other was moved downstream, and the line joining the wires made an angle of 5° with the mean flow velocity. This was done in order to avoid interference effects. When the wires were at their closest position, they were laterally separated rather than one behind the other. Appropriate corrections have been applied to the correlation data by assuming the isotropic relation for the correlation tensor.

Since preliminary measurements showed that the velocity double correlations were unaffected by the presence of temperature fluctuations, the velocity measurements reported here were done with the heat off for convenience.

Temperature double correlations were measured using the hot-wires as resistance thermometers ($i \leqslant 1$ ma). The correlations were corrected for noise by assuming the noise uncorrelated with the signal.

4934

For convenience, the u' spectrum was measured without heating after it had been determined that the u' levels and correlations were not appreciably changed by the heating.

The temperature spectrum was measured with "mixed" sensitivity, that is, wire temperature set for the same order of response to velocity and temperature. This was done because, under pure-resistance-thermometer operation, the signal was inconveniently low at the higher frequencies. Of course, increasing the wire temperature does not increase the rate of gathering of information on the larger voltage signal.

4934

With mixed sensitivity the hot-wire responds to both velocity and temperature spectra, which must be separated. Simple superposition of the two energy spectra follows from the assumption that all harmonics of the two spectra are uncorrelated. Since $\overline{\theta u} \approx 0$ in this field, such an assumption seems reasonable. Then the temperature spectrum is obtained by subtracting the (unheated grid) velocity spectrum from the mixed spectrum.

The skewness of the velocity spatial derivative was determined by differentiating the velocity signal with respect to time and measuring the mean cube and mean square of the resulting signal. The proportionality of instantaneous space and time derivatives is close for this flow (refs. 10 and 11). Since the noise was uncorrelated with the derivative signal, the noise power could be subtracted directly from the mean-square signal. The noise skewness was measured and found equal to zero so that no correction was made to the cubed signal.

The triple velocity correlation measured in this experiment was $k(r)$ since $k(r)$ requires hot-wires sensitive only to u velocity. The wire locations are, of course, identical to those required to measure $p(r)$.

To measure $\overline{u_1^2 u_2(\xi)}$ the signals from two hot-wires, separated a distance $\xi = r$, were subtracted and cubed. The resulting signal, when assuming identical hot-wires, is proportional to

$$u_1^3 - u_2^3 + 3u_1 u_2^2 - 3u_1^2 u_2$$

If the sum of the two signals is also cubed, the result is

$$u_1^3 + u_2^3 + 3u_1 u_2^2 + 3u_1^2 u_2$$

For isotropic turbulence, $\overline{u_1^2 u_2(\xi)}$ is an odd function of ξ so that

$$\overline{u_1^2 u_2} = - \overline{u_2^2 u_1}$$

Also

$$\overline{u_1^3} = \overline{u_2^3} = 0$$

Therefore, if isotropy is assumed, the difference signal is just $6\overline{u_1^2 u_2}$, the desired quantity, and the sum is identically zero. When the sum was measured for the wires in their closest position, however, it was found that the mean cube of the signal was eight times the mean cube of a single-wire voltage. This anomalous behavior was traced to the nonlinear distortion of the signal by the hot-wire itself. The analysis of this situation is given in the appendix.

When the difference of the two voltages is used, the nonlinear hot-wire effect on the mean cube is considerably smaller, a phenomenon similar to the canceling of second-harmonic distortion by a push-pull amplifier. Therefore, all measurements of the correlation $\overline{u_1^2 u_2}$ reported here are measured by using the difference signal only.

The function $S_{\Delta u}(r)$, defined as $\overline{(u_1 - u_2)^3} \Big/ \left[\overline{(u_1 - u_2)^2}\right]^{3/2}$ for $\xi = r$, was obtained by direct measurement of the two factors. At $r = 0$, both numerator and denominator go to zero but in such a way that their ratio is equal to the skewness of the derivative (ref. 2). Therefore, $S_{\Delta u}(0) \equiv S_{\dot{u}}$ was obtained by direct differentiation of the velocity signal.

The cube of the difference signal from two wires adjusted to be equally sensitive to velocity and temperature fluctuations is given by

$$\begin{aligned}\overline{(e_1 - e_2)^3} = {} & \overline{u_1^3} - \overline{u_2^3} + 3\overline{u_2^2 u_1} - 3\overline{u_1^2 u_2} + \overline{\theta_1^3} - \overline{\theta_2^3} + 3\overline{\theta_2^2 \theta_1} - 3\overline{\theta_1^2 \theta_2} + \\ & 3\overline{u_1 \theta_1^2} + 3\overline{\theta_2^2 u_1} - 6\overline{u_1 \theta_1 \theta_2} - 3\overline{u_2 \theta_1^2} - 3\overline{u_2 \theta_2^2} + 6\overline{u_2 \theta_1 \theta_2} + \\ & 3\overline{\theta_1 u_1^2} + 3\overline{\theta_1 u_2^2} - 6\overline{\theta_1 u_1 u_2} - 3\overline{\theta_2 u_1^2} - 3\overline{\theta_2 u_2^2} + 6\overline{\theta_2 u_1 u_2} \qquad (1)\end{aligned}$$

With isotropy, all the terms containing the variables at only one point and the velocity to an odd power are zero. There are also the following isotropic relations:

4934

$$\overline{u_2^2 u_1} = -\overline{u_1^2 u_2} \qquad \overline{u_1 \theta_1 \theta_2} = -\overline{u_2 \theta_1 \theta_2}$$

$$\overline{u_1^2 \theta_1} = \overline{u_2^2 \theta_2} \qquad \overline{\theta_1^2 \theta_2} = \overline{\theta_1 \theta_2^2}$$

$$\overline{u_1^2 \theta_2} = \overline{u_2^2 \theta_1} \qquad \overline{\theta_1^3} = \overline{\theta_2^3}$$

$$\overline{u_1 u_2 \theta_1} = \overline{u_1 u_2 \theta_2}$$

The correlation $\overline{u_1 \theta_2^2}$ or $\overline{u_2 \theta_1^2}$ is identically zero for an isotropic, incompressible field just as the pressure velocity correlation is zero (ref. 10). The correlation $\overline{u_1 u_2 \theta_1}$ is equal to $\overline{u_1 u_2 \theta_2}$ since this is one component of a second-order isotropic tensor, solenoidal in one index, just as f and g are even in the pure velocity case. Therefore, continuity gives a relation between the two components, and this relation preserves the symmetry property. The components analogous to g (e.g., $\overline{\theta_1 v_1 v_2}$) are obviously symmetric, and, therefore, $\overline{\theta_1 u_1 u_2}$ is also symmetric in ξ.

With the assumption of isotropy in the field, therefore, the average of the difference voltage cubed is finally reduced to

$$\overline{(e_1 - e_2)^3} = 6\overline{u_2^2 u_1} + 12\overline{u_1 \theta_1 \theta_2} \tag{2}$$

To determine the triple temperature correlation $\overline{\theta_1^2 \theta_2(\xi)}$, the two wires must be sensitive only to θ temperature fluctuations. In this measurement, both the sum and difference signals of the two wires must be cubed. By assuming identical hot-wires, the cube of the sum minus the cube of the difference signal is proportional to

$$\overline{\theta_1^2 \theta_2} \approx \overline{(e_1 + e_2)^3} - \overline{(e_1 - e_2)^3} \tag{3}$$

which is the required correlation.

The preceding analysis assumes identical hot-wires. In practice, this is an extremely difficult condition to meet. It was found much easier to determine the sensitivities of the two wires by actual calibration and to modify the above analysis to account for this difference. The modification is straightforward in the determination of $\overline{u_1^2 u_2}$ and

$\overline{\theta_1^2\theta_2}$; however, in the measurement of $\overline{u_1\theta_1\theta_2}$ the calculations require that each wire be equally sensitive to velocity and temperature fluctuations. This was impossible to accomplish in general, and the measurements of this function contain contributions from correlations neglected by symmetry conditions in the preceding analysis. However, rough estimates of the order of magnitudes of these terms were made, and appropriate corrections have been made.

4934

EXPERIMENTAL RESULTS

The velocity and temperature fluctuation decay curves are plotted in figures 10 and 11, respectively. A typical pair of runs is given for each to indicate the repeatability of the data as well as the equality of hot- and cold-grid flows. The inverse squares are plotted in figures 12 and 13.

The time spectra of θ and u at $x/M = 17.0$ were determined as described in the previous section and are shown in figure 14. These may be considered fair approximations to the one-dimensional longitudinal space spectra, except for the lowest wave number range (ref. 11). Within the experimental precision there is no significant difference. The circuit noise has been subtracted out for both sets of data.

The skewness of the velocity derivative, defined by

$$S_{\dot{u}} \equiv \frac{\overline{\left(\frac{\partial u}{\partial x}\right)^3}}{\left[\overline{\left(\frac{\partial u}{\partial x}\right)^2}\right]^{3/2}}$$

is shown in figure 15 as a function of x/M. For isotropic turbulence, $S_{\dot{u}} = k'''(0)\lambda_g^3$. The curve indicates that it is a slowly increasing function of x with values in the vicinity of 0.4. The nonconstancy may indicate that the Reynolds number of the turbulence was not sufficiently high for $S_{\dot{u}}$ to be determined solely by eddies in the Kolmogoroff inertial subrange (ref. 3); there were contributions from the larger eddies and from those influenced by viscosity. Other comparable data, including some measurements by Batchelor and Townsend at the same Reynolds number behind a grid of lower solidity (ref. 12) and one measurement by Stewart (ref. 13), are included for comparison.

The temperature field was produced by the turbulence-producing grid itself. It was hoped that this method of introducing the temperature fluctuations would not cause a "spotty" condition to be generated.

However, figure 16 shows $S_\theta \equiv \overline{\theta^3}/(\overline{\theta^2})^{3/2}$ as a function of x/M. Although S_θ is small (max. value, ≈ 0.08), this evidence of an initial "pulse" character is quite measurable.

The longitudinal velocity correlations are shown for various values of x/M in figure 17. The definition of this correlation is $f(r) = \frac{\overline{u_1 u_2}}{u_1' u_2'}$ where the subscript 1 denotes spatial location x, y, z and subscript 2 denotes x+r,y,z. Primes on u_1 and u_2 mean root-mean-square value. It is assumed that $f(r)$ is essentially equal to the isotropic correlations of von Kármán and Howarth (ref. 10). If the turbulence were similar in structure at all decay times, a plot of this $f(r)$ against a nondimensional scale proportional to a local characteristic length would collapse all curves into one. It is well established that such is not the case in actual turbulence. For this plot the length selected was the "dissipation scale" or "Taylor microscale," defined by

$$\frac{1}{\lambda_g^2} = -\left(\frac{\partial^2 f}{\partial r^2}\right)_{r=0} = \frac{2}{\lambda_f^2} \tag{4}$$

The λ's used here were obtained by fitting parabolas to the vertices. Independent determination was made via the decay equation valid for isotropic turbulence. This equation is also due to Taylor:

$$\frac{d\overline{u^2}}{dt} = -10\nu \frac{\overline{u^2}}{\lambda_g^2}$$

and with the use of Taylor's hypothesis for the interchangeability of space and time on the average:

$$\frac{d\overline{u^2}}{dx} = -10 \frac{\nu}{\overline{U}} \frac{\overline{u^2}}{\lambda_g^2} = -20 \frac{\nu}{\overline{U}} \frac{\overline{u^2}}{\lambda_f^2} \tag{5}$$

Therefore, λ_g can be deduced from the decay curve for $\overline{u^2}$ as a function of x. The λ_f comparison is given in figure 18, along with one value obtained from the second moment of the measured power spectrum (ref. 2):

$$\frac{1}{\lambda_f^2} = \frac{1}{2} \int_0^\infty \kappa_x^2 E_u(\kappa_x) d\kappa_x \tag{6}$$

4934 CP-2 back

Within the experimental scatter, the use of r/λ_f collapses the correlations in the region near the origin but not at the tails, consistent with earlier experimental results. The systematic decrease of the correlation with decay time at a fixed r/λ_f shows the well known fact that the turbulence is not accurately similar; still, it is roughly so.

The temperature double correlations

$$m(r) = \frac{\overline{\theta_1 \theta_2}}{\theta_1' \theta_2'}$$

were plotted (fig. 19) in the same way as the velocity correlations but against r/λ_θ, where this thermal "microscale" is given by (ref. 4)

$$\frac{1}{\lambda_\theta^2} = \frac{1}{2}\left(\frac{\partial^2 m}{\partial r^2}\right)_{r=0} \tag{7}$$

That the temperature fluctuation field was reasonably isotropic is evidenced by the approximate equality of the longitudinal and lateral temperature double correlations (fig. 19(b)).

The isotropic temperature decay equation gives an independent estimate of λ_θ (ref. 4):

$$\frac{d\overline{\theta^2}}{dx} = -12 \frac{\gamma}{\overline{U}} \frac{\overline{\theta^2}}{\lambda_\theta^2} \tag{8}$$

The λ_θ scales are compared in figure 18 along with those (ref. 5) computed from the temperature spectrum by an equation like (6).

Figure 20 shows a typical contrast between $f(r)$ and $m(r)$ at the same station. Although $\lambda_\theta \approx \lambda_f$, which corresponds to rough equality of vertex curvatures, $m(r)$ runs higher immediately thereafter, which indicates that

$$m^{iv}(0) > f^{iv}(0) \tag{9}$$

The experimental curves for the triple velocity correlations are shown in figure 21. The values of $k(r)$ were always negative for the x/M and r values covered. According to isotropic turbulence theory, the triple correlation is zero at the origin, rises with an initial cubic variation, and is zero at $r = \infty$. The signal fluctuation made it impractical to measure at large r where $k \approx 0$. Whether $k(r)$ changes

4934

sign or goes to zero with a negative power greater than -4 (ref. 2) cannot be determined from these data.

Figure 22 shows mixed temperature-velocity correlation coefficient at two of the x/M values where the triple velocity correlations were measured. As measured,

$$p(r) = \frac{\overline{u_1 \theta_1 \theta_2}}{\overline{u_1' \theta_1' \theta_2'}} \tag{10}$$

These data are somewhat more scattered than those of $k(r)$. When a correlation function was measured several times, there sometimes occurred systematic differences attributed partly to the inevitable difference between any two hot-wires. Furthermore, individual wire properties change as the wire is used, mainly because of the accumulation of dirt from the airstream.

As shown previously, under the assumption of isotropy it is possible to get $p(r)$ without knowing anything except $k(r)$ if the wires are identical and have their velocity and temperature sensitivities equal. In practice, however, if the inevitably nonidentical wires are operated so that they have the same sensitivity to velocity, their temperature sensitivities will be different. This condition necessitates measurement of other correlations (such as $\overline{\theta_1^2 \theta_2}$) in order to obtain $p(r)$. Estimates were made of these corrections to $p(r)$ and were negligible for the three stations presented. (The correlation $\overline{\theta_1^2 \theta_2}$ was available from a separate measurement.)

The temperature-velocity correlation coefficients have a shape similar to that of the velocity correlations and are of the same order of magnitude. They were negative for all x/M and r studied.

Figures 21 and 22 show the triple correlation behavior as a function of decay time. These curves are plotted against an abscissa scale selected to collapse the curves in the neighborhood of the origin. Analysis, if the fields are considered as isotropic, shows that the velocity correlation starts in the well known way:

$$k(r) = \frac{S_u}{\lambda_g^3} \frac{r^3}{3!} + \cdots \tag{11}$$

and that

$$p(r) \approx \frac{1}{\overline{u'\theta^2}} \overline{\left(\frac{\partial\theta}{\partial x}\right)^2 \left(\frac{\partial u}{\partial x}\right)} \frac{r^3}{3!} + \cdots \tag{12}$$

Therefore, since $S_{\dot{u}}$ is roughly constant, $k(r)$ plotted against r/λ_f should be universal near the origin. Whether $p(r)$ should be a universal function of $r(\lambda_f\lambda_\theta^2)^{-1/3}$ for $r \to 0$ is determined by whether $\frac{\lambda_\theta^2\lambda_f}{\overline{u'\theta^2}} \overline{\frac{\partial u}{\partial x}\left(\frac{\partial\theta}{\partial x}\right)^2}$ is roughly a constant as is the skewness factor of $\partial u/\partial x$. The plots indicate that $\frac{\lambda_\theta^2\lambda_f}{\overline{u'\theta^2}} \overline{\frac{\partial u}{\partial x}\left(\frac{\partial\theta}{\partial x}\right)^2}$ increased more rapidly with decay time than $S_{\dot{u}}$. The quantity $\overline{\frac{\partial u}{\partial x}\left(\frac{\partial\theta}{\partial x}\right)^2}$ was not measured directly because of the loss of the signal in the tube noise.

It appears from figure 23 that p_{max} increased with increasing x/M for the Reynolds and Peclet numbers of this experiment. The peak values of $k(r)$ also increase in absolute value for increasing x/M in agreement with the result of Stewart (ref. 13). Near the origin they fall into one curve, a necessary consequence of the relative constancy of $S_{\dot{u}}$. This is evidenced in figure 21(a) where equation (11) has been computed and plotted.

Plotted in this fashion the tails of neither p nor k are universal functions, which again shows that the fields do not remain similar at different decay times.

Figure 24 shows the function

$$S_{\Delta u}(r) = \frac{\overline{(u_1 - u_2)^3}}{\left[\overline{(u_1 - u_2)^2}\right]^{3/2}} \tag{13}$$

at several x/M. This function attains its maximum at $r = 0$ where its value is $S_{\dot{u}}$, the skewness factor of the velocity derivative (ref. 2). It falls off rapidly to about 0.2 and then gradually decreases, presumably to zero. Its behavior, at all x/M covered, is the same. The fact that this function is not a constant is another indication that the Reynolds number of this turbulence was not sufficiently high for a dominant inertial subrange. These measurements agree very well with those of Stewart (ref. 13).

4934

In figure 25 $n(r)$ is shown as a function of r for the three stations examined. Although the scatter in the data is greater in these results than in the other triple correlations presented, the general trend of this correlation is indicated clearly. The required limit, $n(0) \equiv S_\theta$, is substantiated within the accuracy of these experiments.

Figure 26 shows the measured values of $g(r)$. Included for comparison is the function $g(r)$ computed from the well known isotropic relation (ref. 15)

$$g(r) = \frac{1}{2r} \frac{d}{dr} \left[r^2 f(r) \right]$$

4934

The disagreement shown is probably partly due to the inaccuracy associated with any graphical differentiation process, partly because the scale characterizing the turbulence changes for $r > 0$ in the $f(r)$ curve, and, finally, because the turbulence is not precisely isotropic.

ANALYSIS

The theories of isotropic turbulence and of isotropic scalar fluctuations in isotropic turbulence are still unsolved; in fact, they have not even been formulated in a determinate way without recourse to ad hoc postulates. Nevertheless, a number of consequences of isotropy have been inferred, including some particular (and relatively simple) forms of the averaged differential equations. Several of these consequences have been invoked in the preceding section.

Two-point correlation equations are of special interest here. For isotropic fields decaying in time, there are for the vector and scalar fields, respectively (refs. 4 and 14):

$$\frac{\partial}{\partial t} \left(\overline{u^2} f \right) = \left(\overline{u^2} \right)^{3/2} \left(\frac{\partial k}{\partial r} + \frac{4k}{r} \right) + 2\nu \overline{u^2} \left(\frac{\partial^2 f}{\partial r^2} + \frac{4}{r} \frac{\partial f}{\partial r} \right) \tag{14}$$

and

$$\frac{\partial}{\partial t} \left(\overline{\theta^2} m \right) - 2\overline{\theta^2} \left(\overline{u^2} \right)^{1/2} \left(\frac{\partial p}{\partial r} + 2 \frac{p}{r} \right) = 2\gamma \overline{\theta^2} \left(\frac{\partial^2 m}{\partial r^2} + \frac{2}{r} \frac{\partial m}{\partial r} \right) \tag{15}$$

since

$$k(r) = -2h(r)$$

$$h(r) = -\frac{1}{2} k(r)$$

Sufficient data were taken to permit computation of every term in these equations. Since the triple correlations were the least certain experimental results, these measured functions were compared with those obtained from the double correlations by equations (14) and (15).

Figure 27(b) shows a typical comparison for the velocity field. For small r/λ_f the agreement is somewhat less than that of Stewart's data (ref. 13), which are plotted in figure 27(a), but not significantly so. Figure 22(b) gives the comparison for the mixed triple correlation at station $x/M = 32.0$.

4934

The small disagreement is presumably attributable to either lack of isotropy or inaccuracy in the measurement of triple correlations. Since the small structure should be reasonably isotropic even if the large structure is not, the latter reason seems more likely.

If the correlations appearing in the above equations are expanded in a power series around $r = 0$ and the coefficients of the r^0 terms are kept, the so-called "decay equations" result:

$$\frac{d\overline{u^2}}{dt} = -20\nu \frac{\overline{u^2}}{\lambda_f^2} \tag{16}$$

$$\frac{d\overline{\theta^2}}{dt} = -12\gamma \frac{\overline{\theta^2}}{\lambda_\theta^2} \tag{17}$$

The actual experiments are done in steady state behind a grid with the various averaged quantities depending upon x instead of t. Taylor has pointed out, in effect, that, if these vary sufficiently slowly with x, equation (16) can be applied to the grid flow with the substitution $x/\overline{U} = t$. The same holds for equation (17), so that

$$\frac{d\overline{u^2}}{dx} = -20 \frac{\nu}{\overline{U}} \frac{\overline{u^2}}{\lambda_f^2} \tag{18}$$

$$\frac{d\overline{\theta^2}}{dx} = -12 \frac{\gamma}{\overline{U}} \frac{\overline{\theta^2}}{\lambda_\theta^2} \tag{19}$$

These two equations permit calculations of $\lambda_f(x)$ and $\lambda_\theta(x)$ from the experimental data on $u'(x)$ and $\theta'(x)$, as mentioned in the previous section. The faired results are included in figure 18.

Also plotted in figure 18 are the values of λ obtained graphically from the double correlation curves according to

$$\frac{1}{\lambda_\theta^2} = -\frac{m''(0)}{2} \tag{20}$$

$$\frac{1}{\lambda_f^2} = -\frac{f''(0)}{2} \tag{21}$$

and those calculated from the power spectra.

Reference 1 shows that for two special "kinds" of isotropic fields the ratio λ_θ/λ_f has the same simple value:

$$\frac{\lambda_\theta}{\lambda_f} \approx \sqrt{\frac{1}{Pr}} \tag{22}$$

where Pr is the Prandtl number ν/γ. The two kinds of isotropic fields are:

(1) Reynolds and Peclet numbers are so small that the convective effects are negligible for both heat and momentum. Therefore, this is not really turbulence in the ordinary sense.

(2) Reynolds and Peclet numbers are both very large, and each field is assumed to have completely "self-preserving" correlation function during decay. In this model proposed by von Kármán (ref. 15), the dissipation and conduction terms of the two correlation equations are neglected, but decay is included indirectly by substitution of the decay equations into the terms of the correlation equation.

Equation (22) can also be deduced by an approach somewhat different from the previous:

(3) The Reynolds and Peclet numbers are assumed to be so high that the inertial subranges (with $E_u(\kappa_x)$ and $E_\theta(\kappa_x)$ both $\approx \kappa_1^{-5/3}$) are sufficiently extensive to permit the approximations

$$E_u(\kappa_x) \begin{cases} \approx \kappa_x^{-5/3} & \kappa_0 < \kappa_x < \kappa_c \\ = 0 & \text{elsewhere} \end{cases} \tag{23}$$

4934 CP-3

$$E_\theta(\kappa_x) \begin{cases} \approx \kappa_x^{-5/3} & \kappa_{0,\theta} < \kappa_x < \kappa_{c,\theta} \\ = 0 & \text{elsewhere} \end{cases} \tag{24}$$

The cutoff wave number κ_c is just the inverse of Kolmogoroff's microscale:

$$\kappa_c = \frac{2\pi}{\eta} \tag{25}$$

and $\kappa_{c,\theta}$ is the analogous thermal quantity (ref. 5):

$$\kappa_{c,\theta} = \frac{2\pi}{\eta_\theta} \tag{26}$$

In reference 5 it is shown that

$$\frac{\kappa_{c,\theta}}{\kappa_c} = (Pr)^{3/4} \tag{27}$$

The microscales can be obtained from the second moment of the power spectrum as

$$\frac{1}{\lambda_f^2} = \frac{1}{2}\int_0^\infty \kappa_x^2 E_u(\kappa_x)\,d\kappa_x \tag{6}$$

$$\frac{1}{\lambda_\theta^2} = \frac{1}{2}\int_0^\infty \kappa_x^2 E_\theta(\kappa_x)\,d\kappa_x \tag{28}$$

Substituting equations (23) to (27) into (6) and (28) and neglecting $\kappa_0^{2/3}$ relative to $\kappa_c^{2/3}$ and $\kappa_{0,\theta}^{2/3}$ relative to $\kappa_{c,\theta}^{2/3}$ result in

$$\frac{\lambda_\theta^2}{\lambda_f^2} \approx \left(\frac{\kappa_0}{\kappa_{0,\theta}}\right)^{2/3} \frac{1}{Pr} \tag{29}$$

If consideration is now restricted to fields in which the thermal large eddy structure is roughly equal to the velocity large eddy structure (as in these experiments), $\kappa_0 \approx \kappa_{0,\theta}$, which again results in equation (22).

4934

In fact, none of the three sets of assumptions leading to equation (22) is directly applicable to these experiments. The Reynolds and Peclet numbers are not low enough for case (1) and not high enough for the other two cases. Furthermore, it was shown that the correlation functions of velocity do not remain completely similar during decay. The important conjecture to be made is that a result encountered under such divergent sets of assumptions may have approximate validity in a wide range of situations, perhaps including the actual one.

By taking $Pr = 0.72$ for air, equation (22) gives

$$\frac{\lambda_\theta}{\lambda_f} \approx 1.2 \tag{30}$$

which is in reasonable agreement with the downstream values of λ_θ/λ_f computed from the decay curves but is higher than the values computed from the correlations. The data indicate a trend toward satisfaction of this relation for large decay times. The only other measurement of this ratio was on the axis of a heated round turbulent jet (ref. 8), where the value was 0.95.

The solid λ_θ/λ_f curve in figure 18 is just a particular way of displaying the decay data. Two other ways are also instructive. Figure 28 shows the variation in Reynolds and Peclet numbers:

$$\left.\begin{aligned} Re &\equiv \frac{u'\lambda_g}{\nu} \\ Pe &\equiv \frac{u'\lambda_\theta}{\gamma} \end{aligned}\right\} \tag{31}$$

with λ taken from the decay data. The apparent constancy of Pe is evident.

Figure 29 shows the relative decay rates of temperature and velocity fluctuations. For small x/M, these fluctuations die out at about the same rate, but, for larger x/M, θ' dies out at a decidedly lower rate than does u'. For fully isotropic fields the ratio of equation (19) to equation (18) gives

$$\frac{\frac{d\theta'}{\theta'}}{\frac{du'}{u'}} = \frac{6}{10(Pr)}\left(\frac{\lambda_f}{\lambda_\theta}\right)^2 \tag{32}$$

4934 CP-3 back

and, if equation (22) holds,

$$\frac{d\theta'}{\theta'} \quad \frac{u'}{du'} = \frac{3}{5} \tag{33}$$

which is very close to the measured results at large x/M. Notice that equation (33) is independent of Pr.

No attempt has been made to compare the individual decay rates of θ' and u' with the theoretical predictions that can be obtained by a variety of postulates.

The integral scales are defined by

$$\left.\begin{aligned} L_f &= \int_0^\infty f(r)\,dr \\ \text{and} \qquad L_\theta &= \int_0^\infty m(r)\,dr \end{aligned}\right\} \tag{34}$$

These are shown in figure 30. Reference 4 shows that, with self-preserving correlations, if the scales are equal at any instant and also at the initial time, they will remain equal. The small discrepancy here is doubtless a result of the fact that there is certainly no complete similarity in either field. Another consequence of a supposed similarity in both fields is that

$$\left.\begin{aligned} \frac{\lambda_\theta}{L_\theta}\,Pe &= \text{const.} \\ \text{and that} \qquad \frac{\lambda}{L_f}\,Re &= \text{const.} \end{aligned}\right\} \tag{35}$$

Figure 31 shows good agreement with both relations for large decay times.

Figure 23 shows the value of k_{max} as a function of decay time, contrasted with the results of Stewart (ref. 12). It is interesting to speculate on the history of k_{max} for even greater decay times. A monotonic increase in k_{max} (toward unity) would not be in contradiction to the usual approximations for very large decay time, that is, the so-called "final period" results, because the coefficient of the k term of the correlation equation is the factor which certainly becomes negligible as $Re \to 0$. It seems plausible, though, that in the limiting case of

4934

random Stokes' flow, analogous to heat conduction in a solid medium, the velocity probability density is symmetrical, in which case $k(r)$ would go to zero at $t \to \infty$.

CONCLUDING REMARKS

In roughly isotropic concomitant velocity and temperature fluctuation fields it has been found that:

1. The temperature fluctuations die out more slowly than the turbulence (fig. 29) in approximate agreement with the predictions of reference 4.

2. The temperature double correlation coefficient function is roughly equal to the "longitudinal" velocity correlation.

3. The "mixed" triple correlation coefficient function entering the double temperature correlation equation is of the same order as the corresponding velocity triple correlation.

More explicit statement of detailed quantitative results covered herein will not be given here because these results may not have sufficient universality. They may be significantly characteristic of the deviations from isotropy in these velocity and temperature fields.

The Johns Hopkins University,
Baltimore, Md., June 12, 1957.

APPENDIX - EFFECT OF HOT-WIRE NONLINEARITY ON TRIPLE CORRELATION MEASUREMENT

At "small" fluctuation levels, perhaps $u'/\overline{U} < 10$ percent, the Dryden-Kuethe linearized equation for hot-wire response (ref. 16) is satisfactory for measurements of a number of turbulence properties. For example, it is well known that turbulence level, double correlation, and power spectrum measurements are not seriously distorted in the (< 3-percent level) isotropic turbulence rather far behind a grid. However, previous research (ref. 13) makes no mention of this possible source of error in triple correlation measurements. It is evident that this replacement of the response curve by its local tangent will lead to poorer approximations for functions which depend more heavily on the tails of the probability density of $u(t)$. Furthermore, away from response curve inflection points it seems evident that odd moments will tend to fare worse under linear approximation than will even ones.

The simplest case of concern here is the skewness of u, $S_u \equiv \overline{u^3}/(\overline{u^2})^{3/2}$. A first-order estimate of the error in this measurement is obtained by keeping the parabolic terms in the perturbation form of King's equation for hot-wire sensitivity. A suitable approximate form of King's equation is

$$\frac{i^2 R_a}{R - R_a} = A - i^2 + B\sqrt{U} \tag{A1}$$

where

A,B constants

i wire current, taken constant here

R wire resistance

R_a wire resistance at ambient fluid temperature, taken constant here

U instantaneous velocity normal to wire

Writing $U = \overline{U} + u$ and $R = \overline{R} + r$ where $\overline{u} = \overline{r} \equiv 0$ and expanding the square root out to u^2 give

$$R = \overline{R} + r \approx R_a + \frac{i^2 R_a}{A - i^2 + B\sqrt{\overline{U}}}\left[1 - \frac{B\sqrt{\overline{U}}}{A - i^2 + B\sqrt{\overline{U}}}\left(\frac{u}{\overline{U}}\right) + \frac{1}{8}\frac{B\sqrt{\overline{U}}}{A - i^2 + B\sqrt{\overline{U}}}\left(1 + \frac{2B\sqrt{\overline{U}}}{A - i^2 + B\sqrt{\overline{U}}}\right)\left(\frac{u}{\overline{U}}\right)^2\right] \tag{A2}$$

Averaging equation (A2) and subtracting the average from (A2) result in

$$e \equiv ir \approx \frac{i^3 BR_a\sqrt{\bar{U}}}{2\left(A - i^2 + B\sqrt{\bar{U}}\right)^2}\left[-\left(\frac{u}{\bar{U}}\right) + \frac{1}{4}\left(1 + \frac{2B\sqrt{\bar{U}}}{A - i^2 + B\sqrt{\bar{U}}}\right)\frac{u^2 - \overline{u^2}}{\bar{U}^2}\right] \tag{A3}$$

4934

from which could be computed the measured skewness,

$$S_e \equiv \frac{\overline{e^3}}{\left(\overline{e^2}\right)^{3/2}}$$

as a function of the true skewness S_u and of other flow and wire properties. For simplicity, the analysis is restricted to isotropic turbulence, in which case $S_u = 0$. The relation $\overline{u^4}/\left(\overline{u^2}\right)^2 = -3$ is taken as the Gaussian value, and the final estimate is

$$S_e \approx \frac{3}{2}\left(1 + \frac{2B\sqrt{\bar{U}}}{A - i^2 + B\sqrt{\bar{U}}}\right)\frac{u}{\bar{U}} \tag{A4}$$

For a typical 0.1-mil platinum wire at an overheat temperature of 50° C in 2-percent turbulence level flow, this estimate gives

$$S_e \approx 0.05$$

even though $S_u = 0$.

The seriousness of this effect can be gauged by observing that 0.05 is the order of the maximum value of the triple correlation coefficient $k(r)$.

Before proceeding to an estimate of the effect on triple correlation measurement, the determination of skewness of velocity derivative is considered:

$$S_{\dot{u}} \equiv \frac{\overline{\left(\frac{\partial u}{\partial t}\right)^3}}{\left[\overline{\left(\frac{\partial u}{\partial t}\right)^2}\right]^{3/2}}$$

Following a procedure similar to that for S_e, an estimate is obtained for $S_{\dot{e}} \equiv \frac{\overline{\left(\frac{\partial e}{\partial t}\right)^3}}{\left[\overline{\left(\frac{\partial e}{\partial t}\right)^2}\right]^{3/2}}$ in isotropic turbulence:

$$S_{\dot{e}} \approx -S_{\dot{u}}\left[1 - \frac{15}{4}\left(C^2 + C + \frac{2}{5}\right)\frac{\overline{u^2\left(\frac{\partial u}{\partial x}\right)^2}}{\overline{U}^2\overline{\left(\frac{\partial u}{\partial x}\right)^2}}\right] \tag{A5}$$

where

$$C \equiv \frac{B\sqrt{\overline{U}}}{A - i^2 + B\sqrt{\overline{U}}}$$

For the typical hot-wire operation cited previously, equation (A5) gives

$$S_{\dot{e}} \approx -S_{\dot{u}}(1 - 0.005)$$

which indicates a negligible effect. The quadruple correlation is estimated from the data of reference 17.

In a completely formal measurement of triple correlation coefficient (using mean cubes of sum and difference voltage) an additive error can be expected of the order of that in S_e, which is appreciable. However, for isotropic turbulence the triple correlation is just proportional to the skewness of the velocity difference (see section on experimental procedure), and it is not difficult to show that in velocity difference skewness measurement the error due to nonlinearity is small. In a sense, the effects of the two wires tend to cancel. Hence, it is convenient for reasons of both speed and reduction of error to follow Townsend in assuming isotropy and thereby using the ideal relation

$$\overline{(u_1 - u_2)^3} = -6\overline{u_1^2 u_2} = -6\left(\overline{u^2}\right)^{3/2} k(r)$$

Writing the two wire responses in series form gives

$$e_1 = \sum_{i=0}^{\infty} a_i u_1^i \qquad e_2 = \sum_{j=0}^{\infty} a_j u_2^j \tag{A6}$$

where a_i and a_j are proportionality constants. Terminated with the u^2 terms, equations (A6) become equation (A3), from which an estimate of

the first-order error committed by assuming that any dimensionless statistical function of e_1, e_2 is equal to the corresponding function of u_1, u_2. In particular, the difference skewness factors $\overline{(e_1 - e_2)^3} \Big/ \left[\overline{(e_1 - e_2)^2}\right]^{3/2}$ and $\overline{(u_1 - u_2)^3} \Big/ \left[\overline{(u_1 - u_2)^2}\right]^{3/2}$ turn out to be related by

$$S_{\Delta e} = S_{\Delta u}\left\{1 - 3\left[\frac{1}{4}\left(C + \frac{1}{2}\right)^2 \frac{\overline{u_1^4} - \overline{u_1^2 u_2^2}}{\overline{U}^2\,\overline{(u_1 - u_2)^2}} - \frac{3}{2}\left(C^2 + C + \frac{1}{2}\right) \frac{\overline{u_1^4} - \overline{u_1^3 u_2}}{\overline{U}^2\,\overline{(u_1 - u_2)^2}}\right] + \text{higher order terms}\right\} \tag{A7}$$

For the example used earlier equation (A7) gives an error of less than 0.2 percent for $r > \frac{1}{2}\lambda$ and rises to perhaps 2 percent at $r \to 0$. Hence, this effect is negligible within the accuracy of these measurements.

In the cubed-difference approximation to triple correlation, the same approach leads to

$$\frac{\overline{(e_1 - e_2)^3}}{\overline{e_1^2}\sqrt{\overline{e_2^2}}} \approx \frac{\overline{(u_1 - u_2)^3}}{\overline{u_1^2}\sqrt{\overline{u_2^2}}}\left[1 - 3\left(C^2 + C + \frac{7}{16}\right)\frac{\overline{u^2}}{\overline{U}^2}\right] \tag{A8}$$

after the assumption of $\overline{u^4}/(\overline{u^2})^2 = 3$. This corresponds to percent errors about 10 times those in $S_{\Delta e}$, but these errors are appreciable only as $r \to 0$ where $\overline{(e_1 - e_2)^3} \Big/ \overline{e_1^2}\sqrt{\overline{e_2^2}}$ is also going rapidly to zero; thus, no difficulty arises.

REFERENCES

1. Taylor, G. I.: Statistical Theory of Turbulence, pts. I-IV. Proc. Roy. Soc. (London), ser. A, vol. 151, no. A873, Sept. 1935, pp. 421-478.

4934 CP-4

2. Batchelor, G. K.: The Theory of Homogeneous Turbulence. Cambridge Univ. Press, 1953.

3. Kolmogoroff, A. N.: The Local Structure of Turbulence in Incompressible Fluid at Very Large Reynolds Numbers. Comp. Rend., vol. XXX, no. 4, 1941, pp. 301-305.

4. Corrsin, S.: The Decay of Isotropic Temperature Fluctuations in an Isotropic Turbulence. Jour. Aero. Sci., vol. 18, no. 6, June 1951, pp. 417-423.

5. Corrsin, S.: On the Spectrum of Isotropic Temperature Fluctuations in an Isotropic Turbulence. Jour. Appl. Phys., vol. 22, no. 4, Apr. 1951, pp. 469-473.

6. Obukhov, A. M. (V. Bartlett, trans.): Structure of the Temperature Field in Turbulent Flow. Trans. from Isvestiia Akad. Nauk SSSR, Geogr. i. Geofis, vol. 13, no. 1, 1949, pp. 58-69.

7. Corrsin, S.: Decay of Turbulence Behind Three Similar Grids. A. E. Thesis, C.I.T., June 1942.

8. Corrsin, Stanley, and Uberoi, Mahinder S.: Spectra and Diffusion in a Round Turbulent Jet. NACA Rep. 1040, 1951. (Supersedes NACA TN 2124.)

9. Corrsin, Stanley: Extended Applications of the Hot-Wire Anemometer. NACA TN 1864, 1949.

10. Lin, C. C.: On Taylor's Hypothesis and the Acceleration Terms in the Navier-Stokes Equation. Quart. Appl. Math., vol. 10, no. 4, Jan. 1953, pp. 295-306.

11. Uberoi, Mahinder S., and Corrsin, Stanley: Diffusion of Heat from a Line Source in Isotropic Turbulence. NACA Rep. 1142, 1953. (Supersedes NACA TN 2710.)

12. Batchelor, G. K., and Townsend, A. A.: Decay of Vorticity in Isotropic Turbulence. Proc. Roy. Soc. (London), ser. A, vol. 190, no. A 1023, Sept. 9, 1947, pp. 534-550.

13. Stewart, R. W.: Triple Velocity Correlations in Isotropic Turbulence. Proc. Cambridge Phil. Soc., vol. 47, pt. 1, 1951, pp. 146-157.

14. Kovasznay, L. S. G.: Development of Turbulence-Measuring Equipment. NACA Rep. 1209, 1954. (Supersedes NACA TN 2839.)

15. von Kármán, Theodore, and Howarth, Leslie: On the Statistical Theory of Isotropic Turbulence. Proc. Roy. Soc. (London), ser. A, vol. 164, Jan. 21, 1938, pp. 192-215.

4934

16. Dryden, H. L., and Kuethe, A. M.: The Measurement of Fluctuations of Air Speed by the Hot-Wire Anemometer. NACA Rep. 320, 1929.

17. Uberoi, Mahinder S.: Correlations Involving Pressure Fluctuations in Homogeneous Turbulence. NACA TN 3116, 1954.

4934

CP-4 back

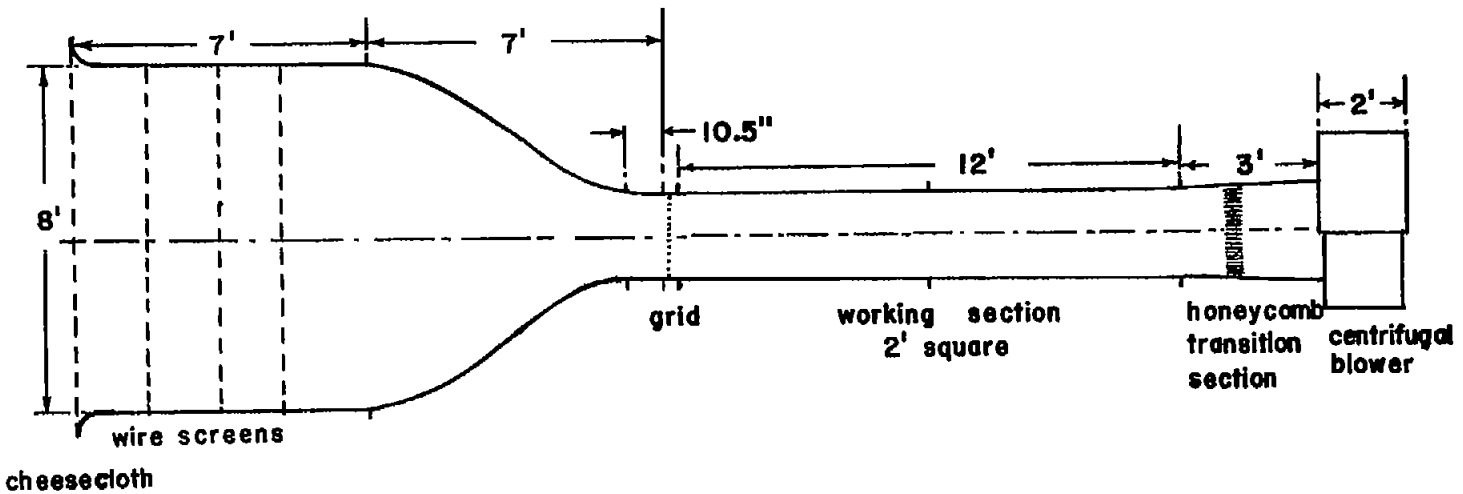

Figure 1. Diagram of test facility.

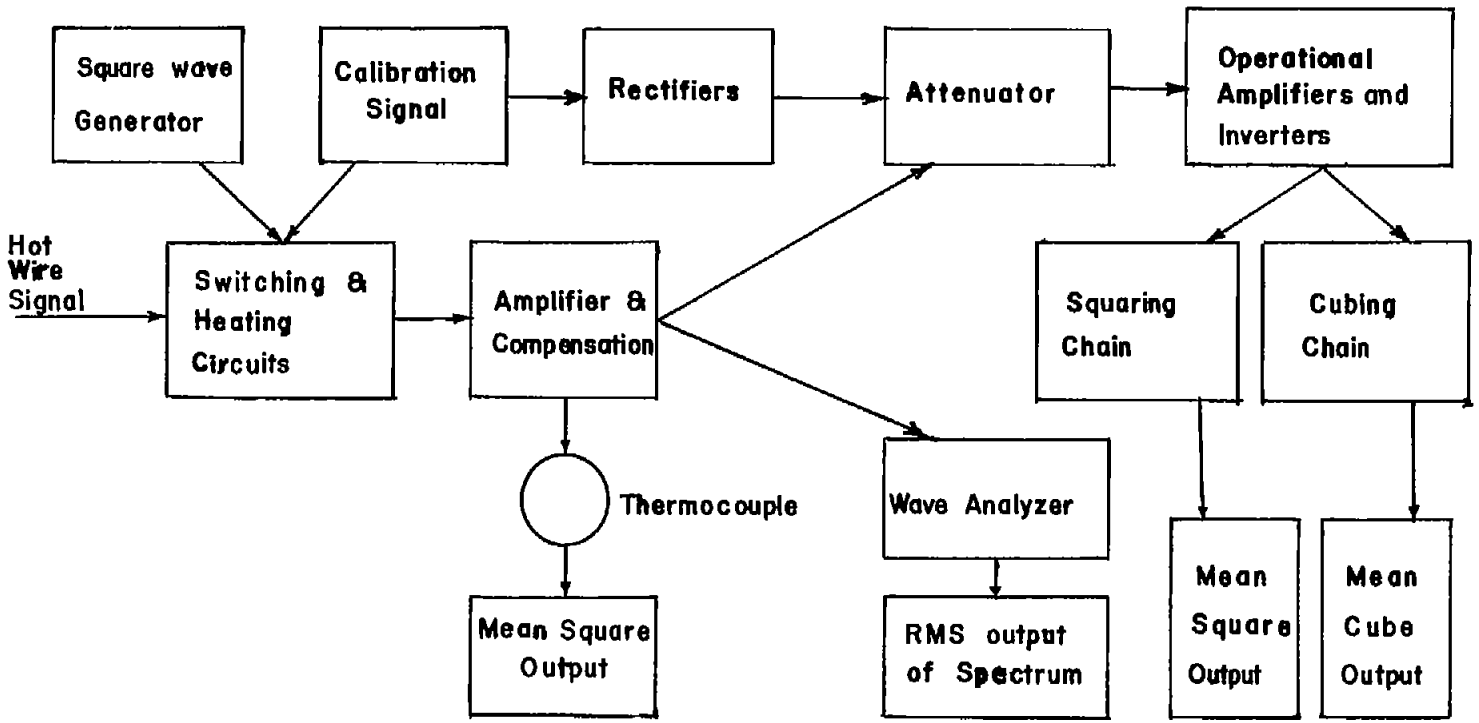

Figure 2. - Block diagram of electronic components.

4934

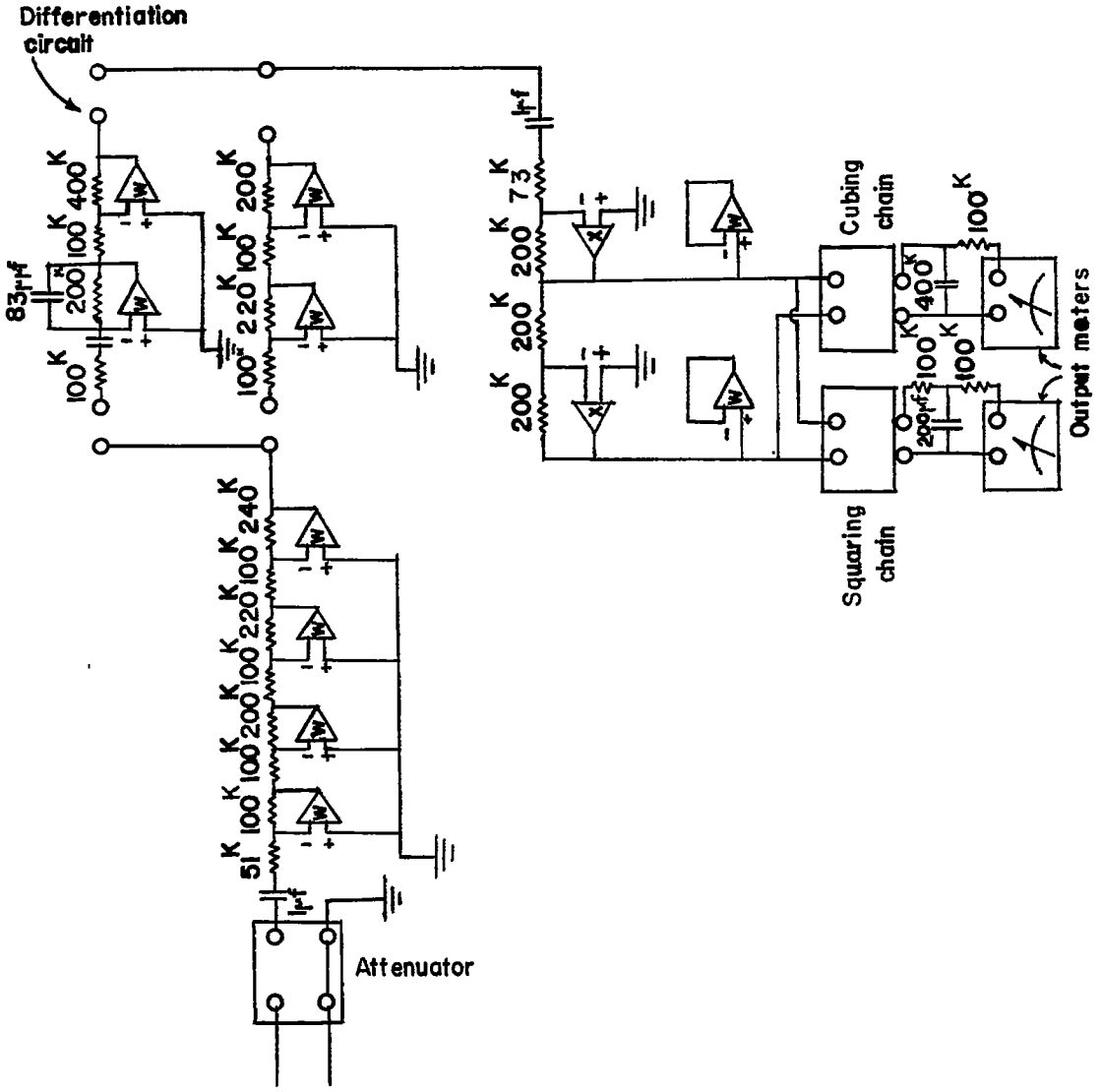

Figure 3. - Operational amplifier components.

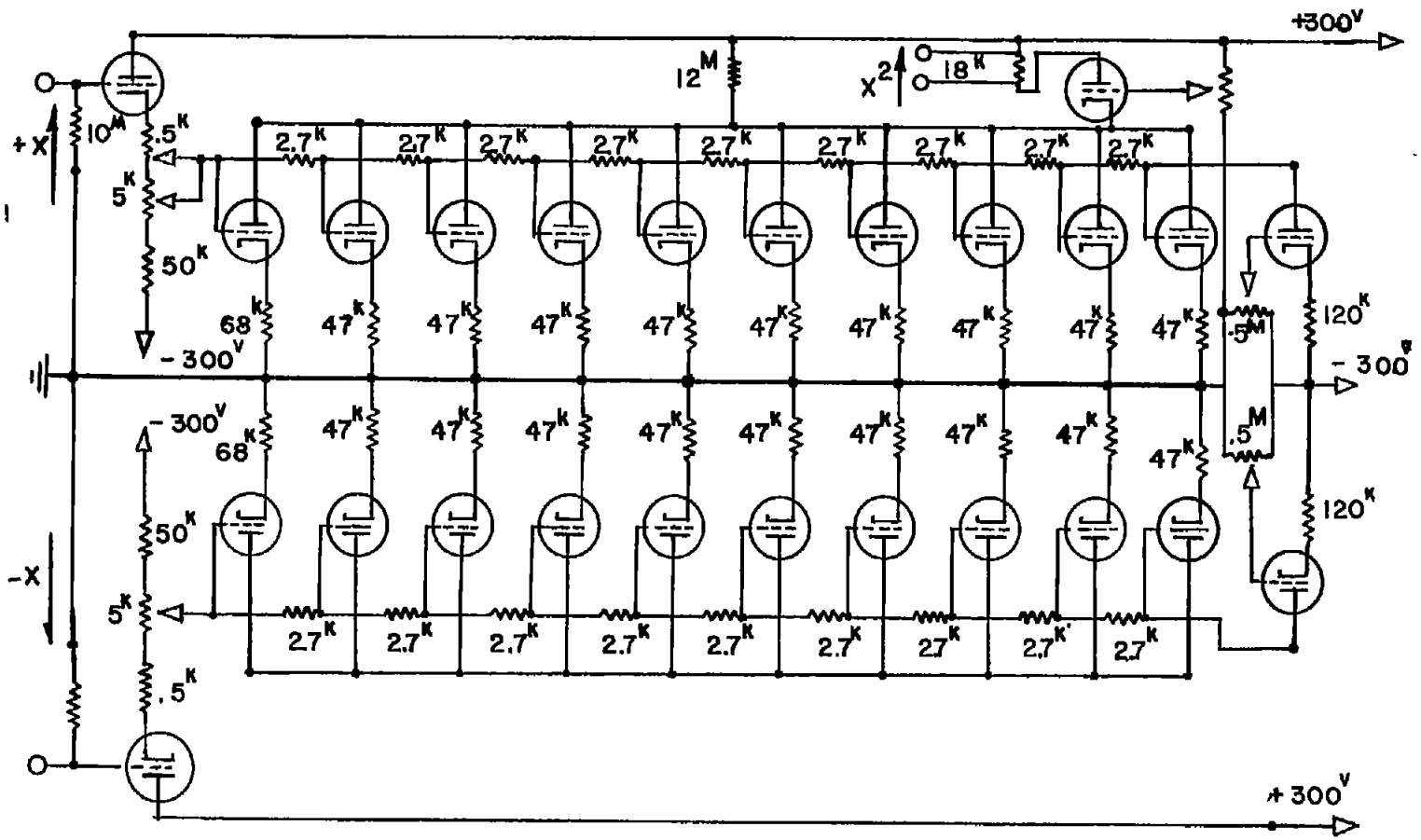

Figure 4. - Squaring circuit. (All tubes 12AT7.)

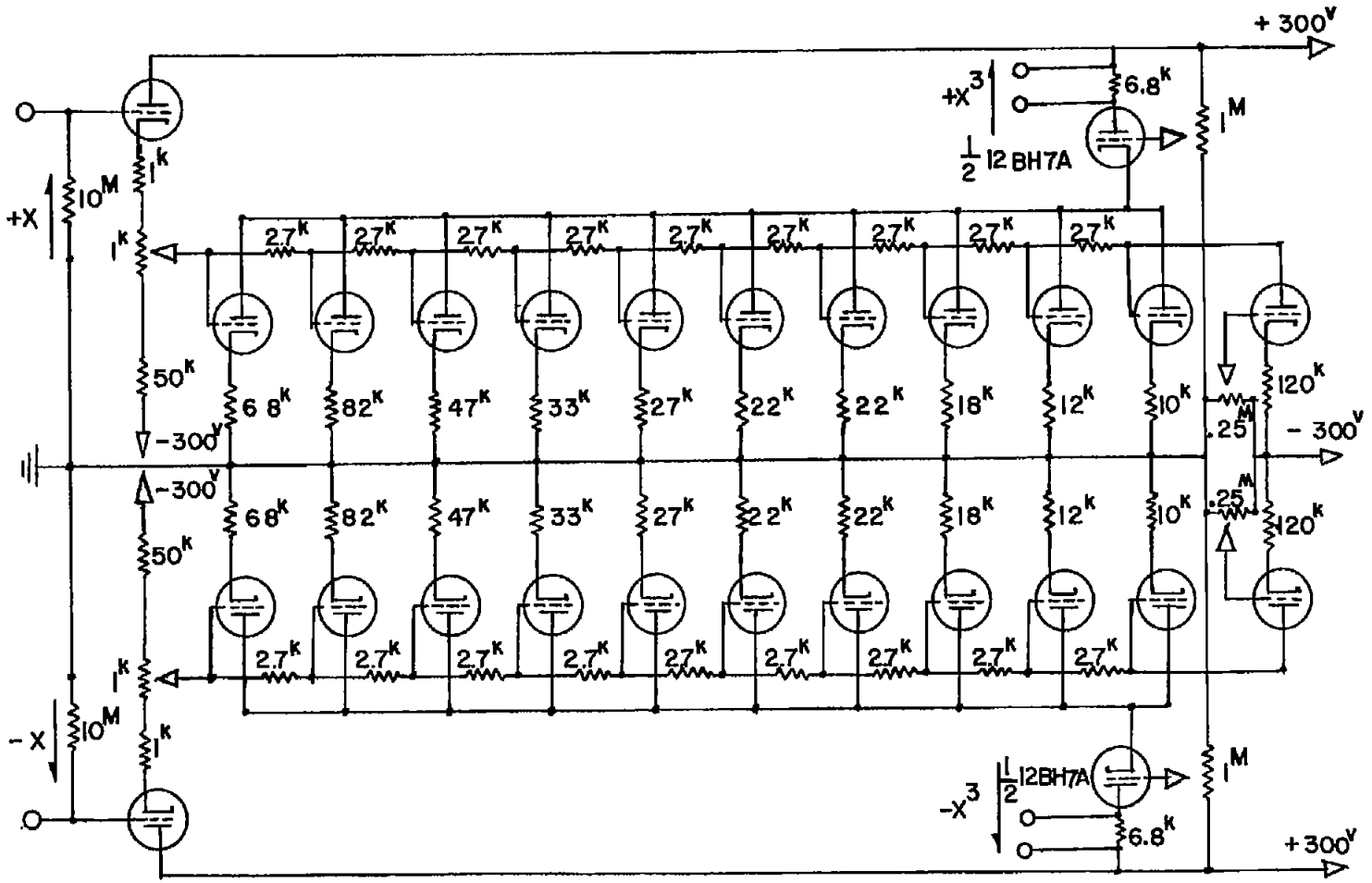

Figure 5. - Cubing circuit. (All tubes 12AT7 except as noted.)

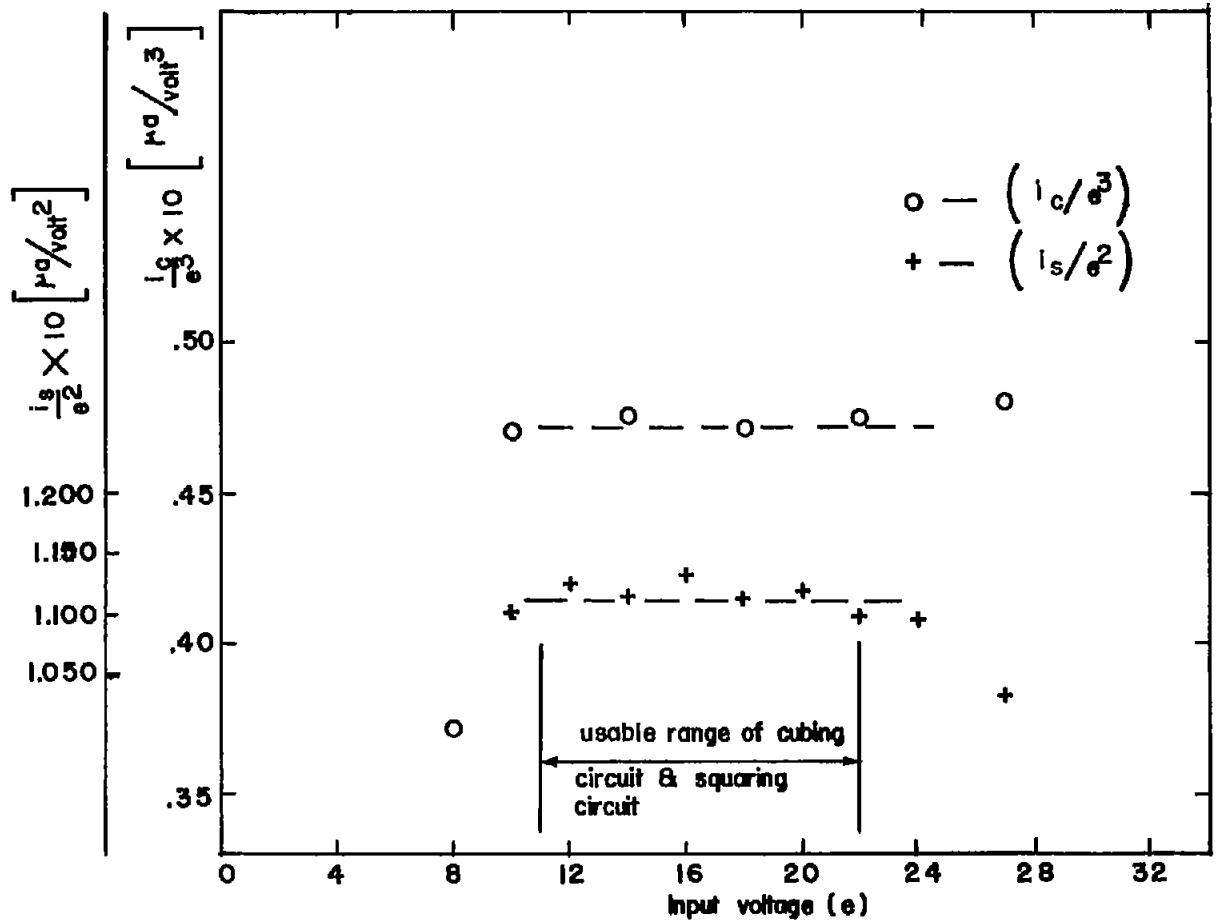

(a) Operational range.

Figure 6. - Typical calibrations of squaring and cubing circuits.

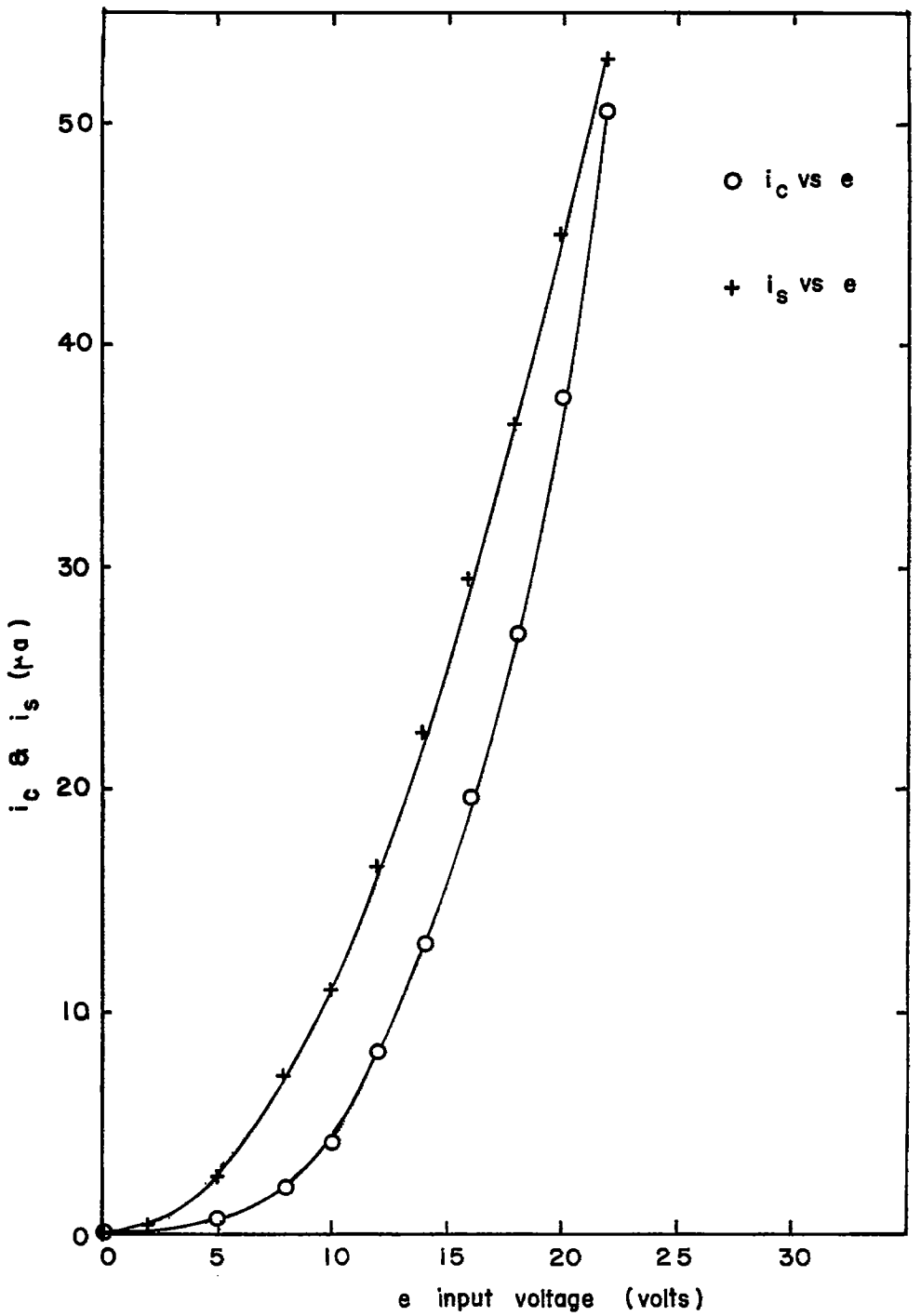

(b) Over-all voltage range.

Figure 6. - Concluded. Typical calibrations of squaring and cubing circuits.

4934

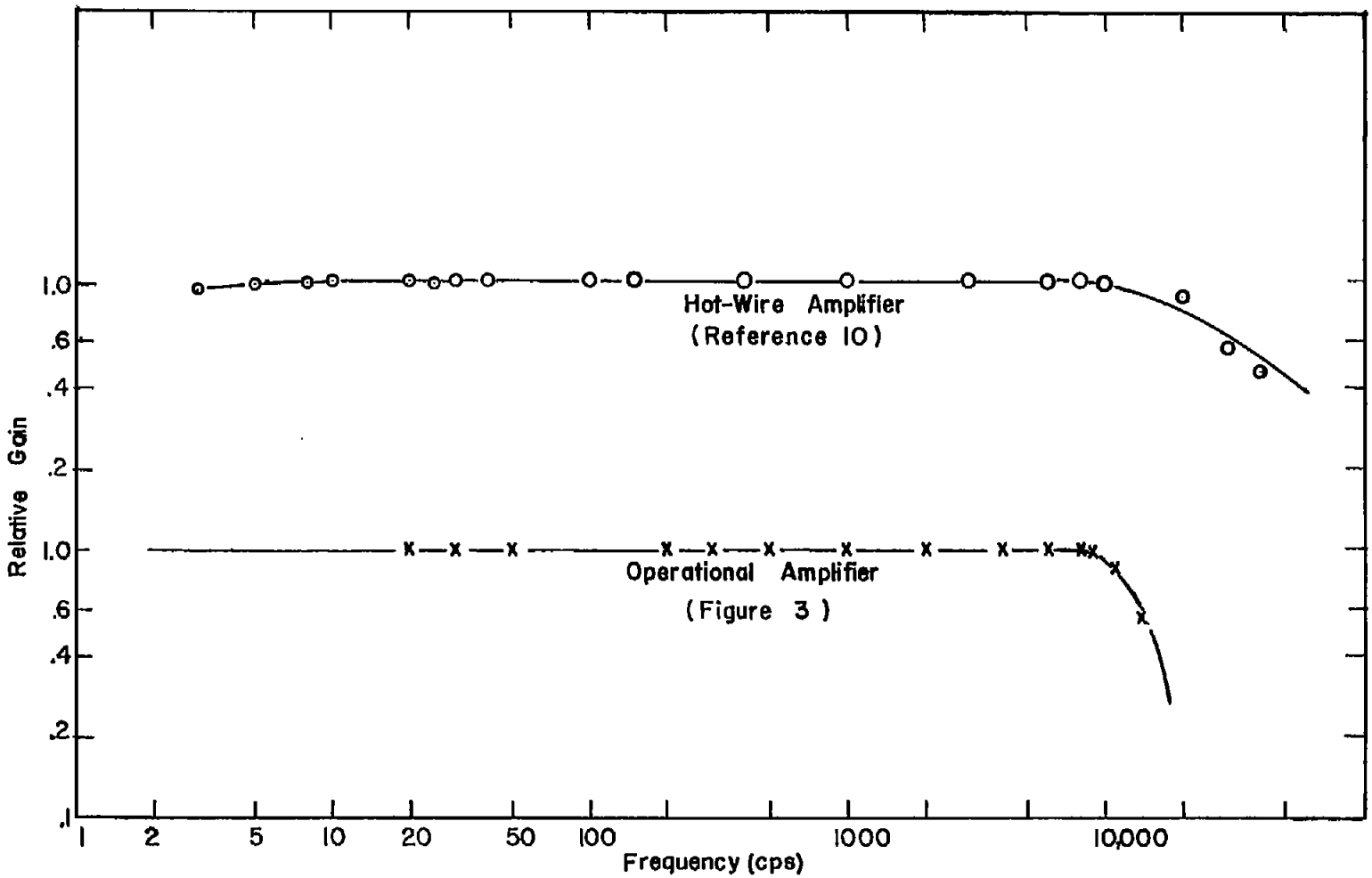

(a) Auxiliary and hot-wire amplifiers.

Figure 7. - Frequency response of measuring equipment.

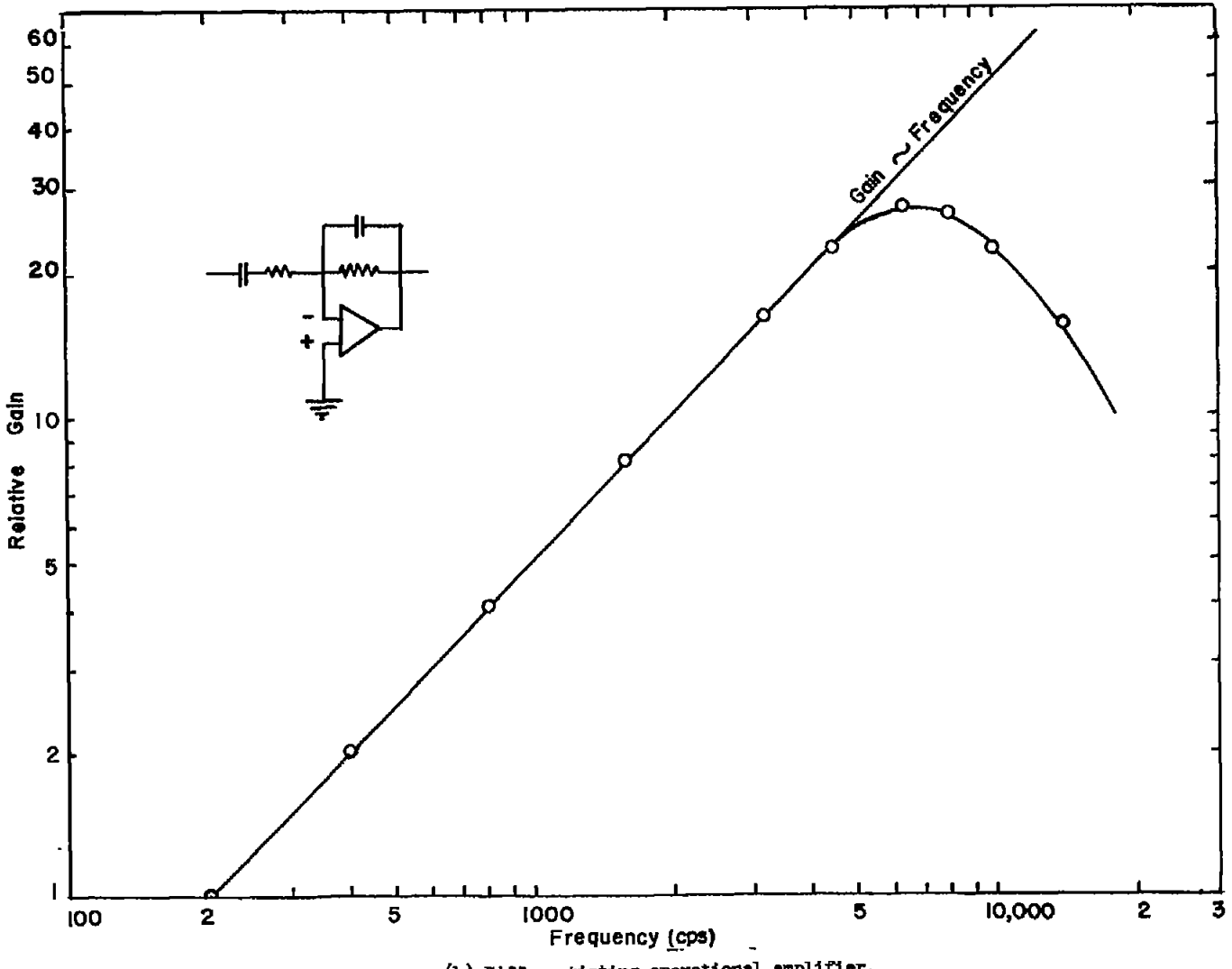

(b) Differentiating operational amplifier.

Figure 7. - Concluded. Frequency response of measuring equipment.

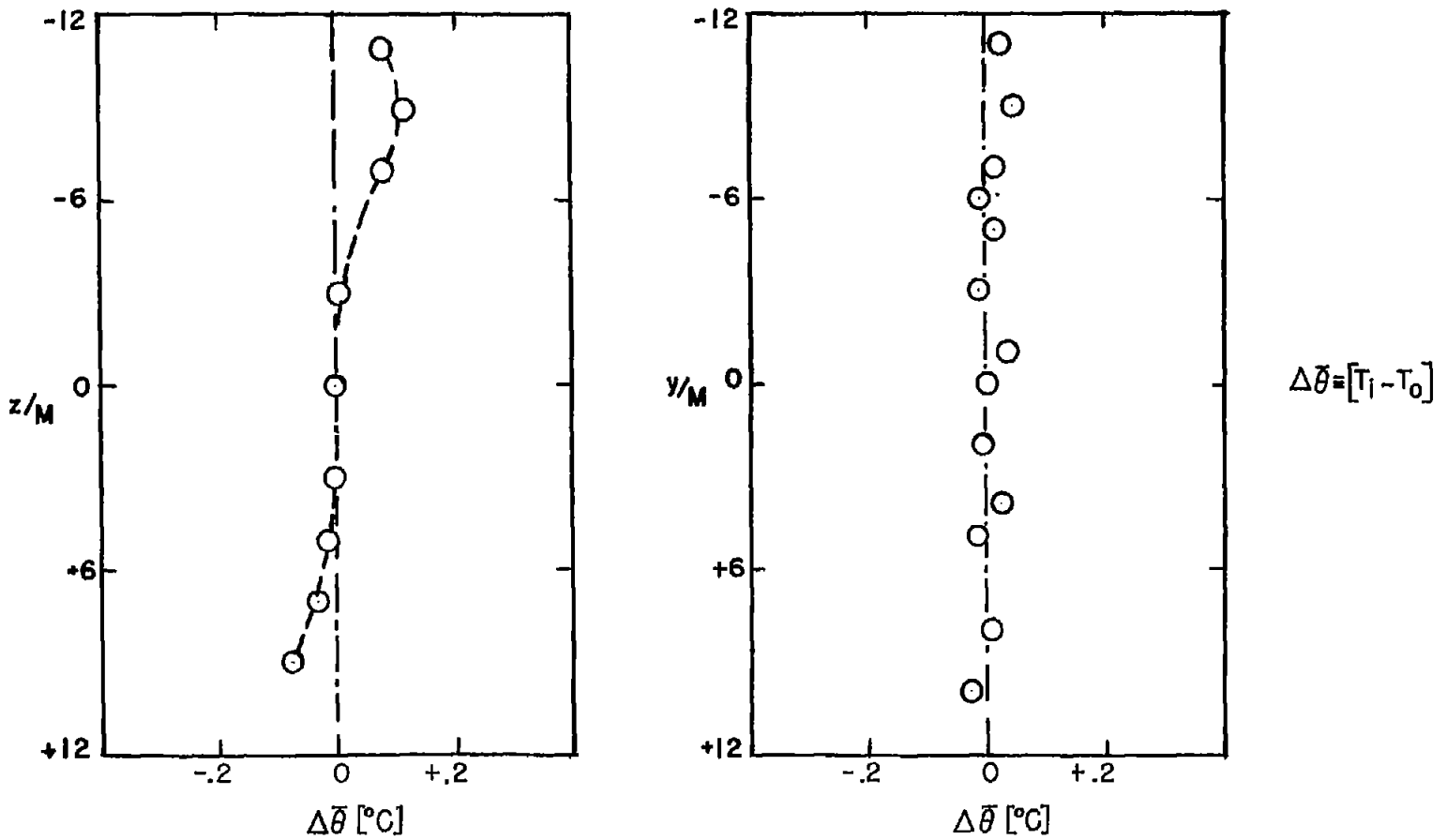

Figure 8. - Mean temperature distribution (vertical and horizontal). x/M = 15.0.

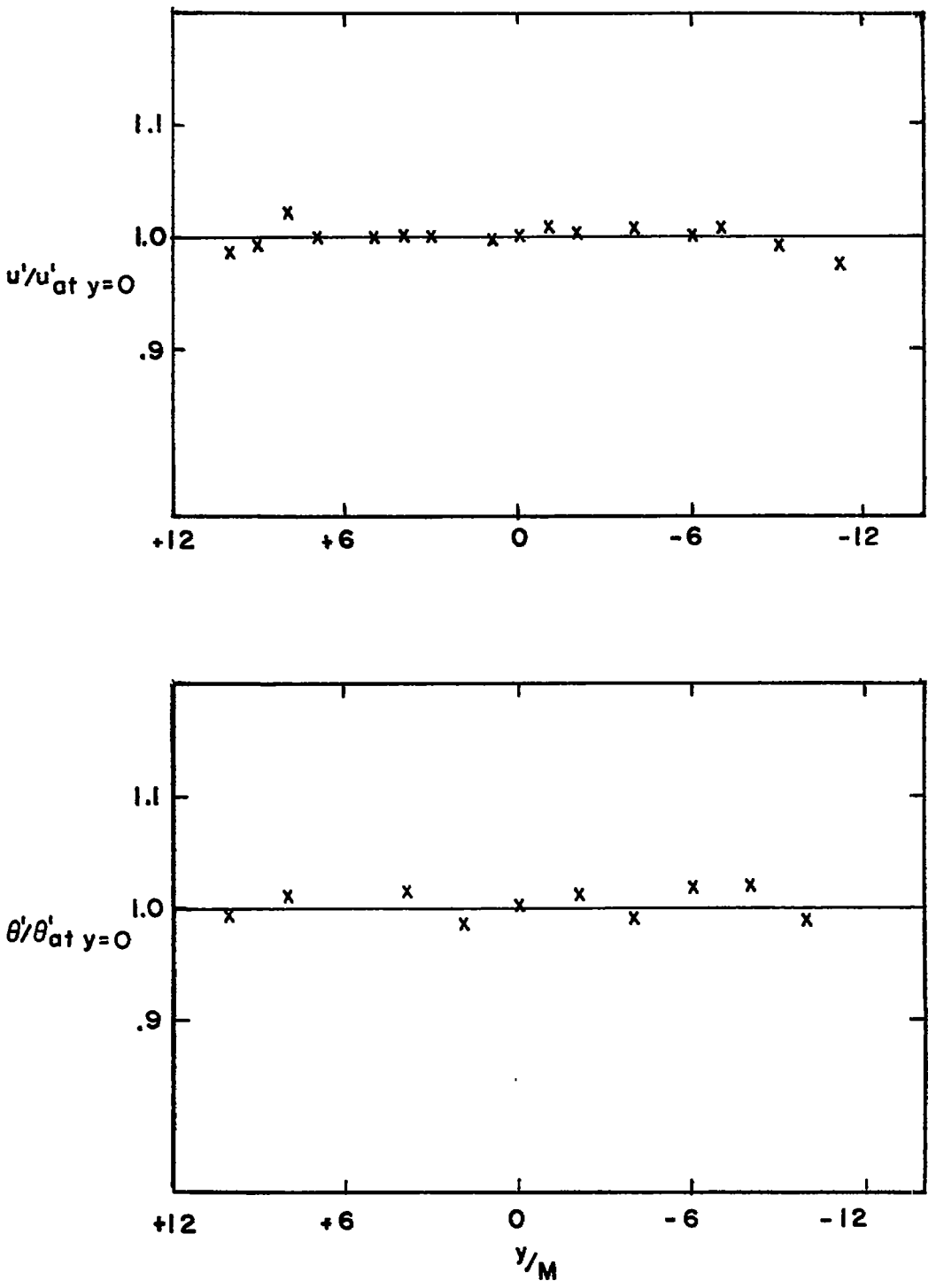

Figure 9. - Homogeneous turbulence and temperature fields.

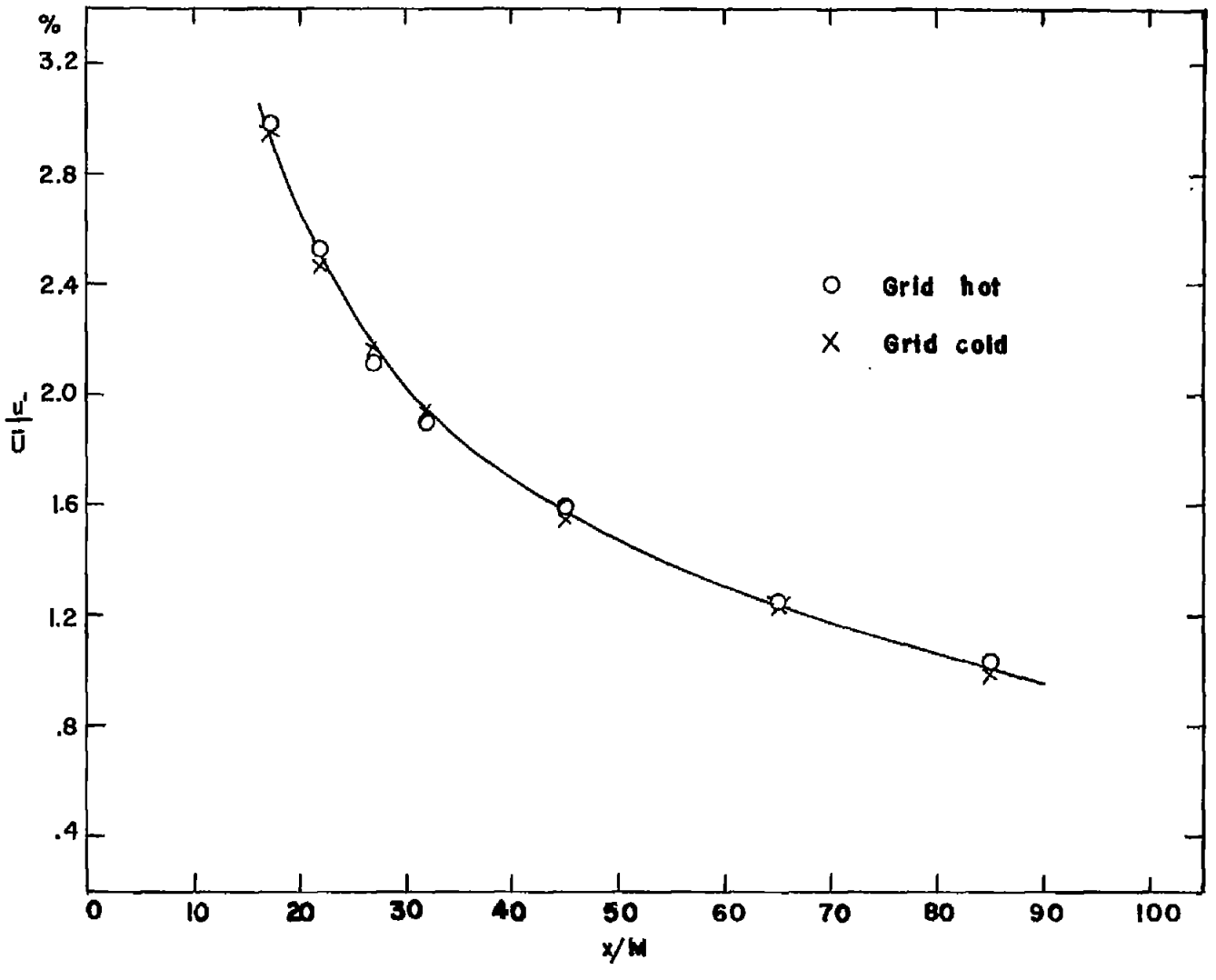

Figure 10. - Longitudinal turbulence decay. R_M = 7420.

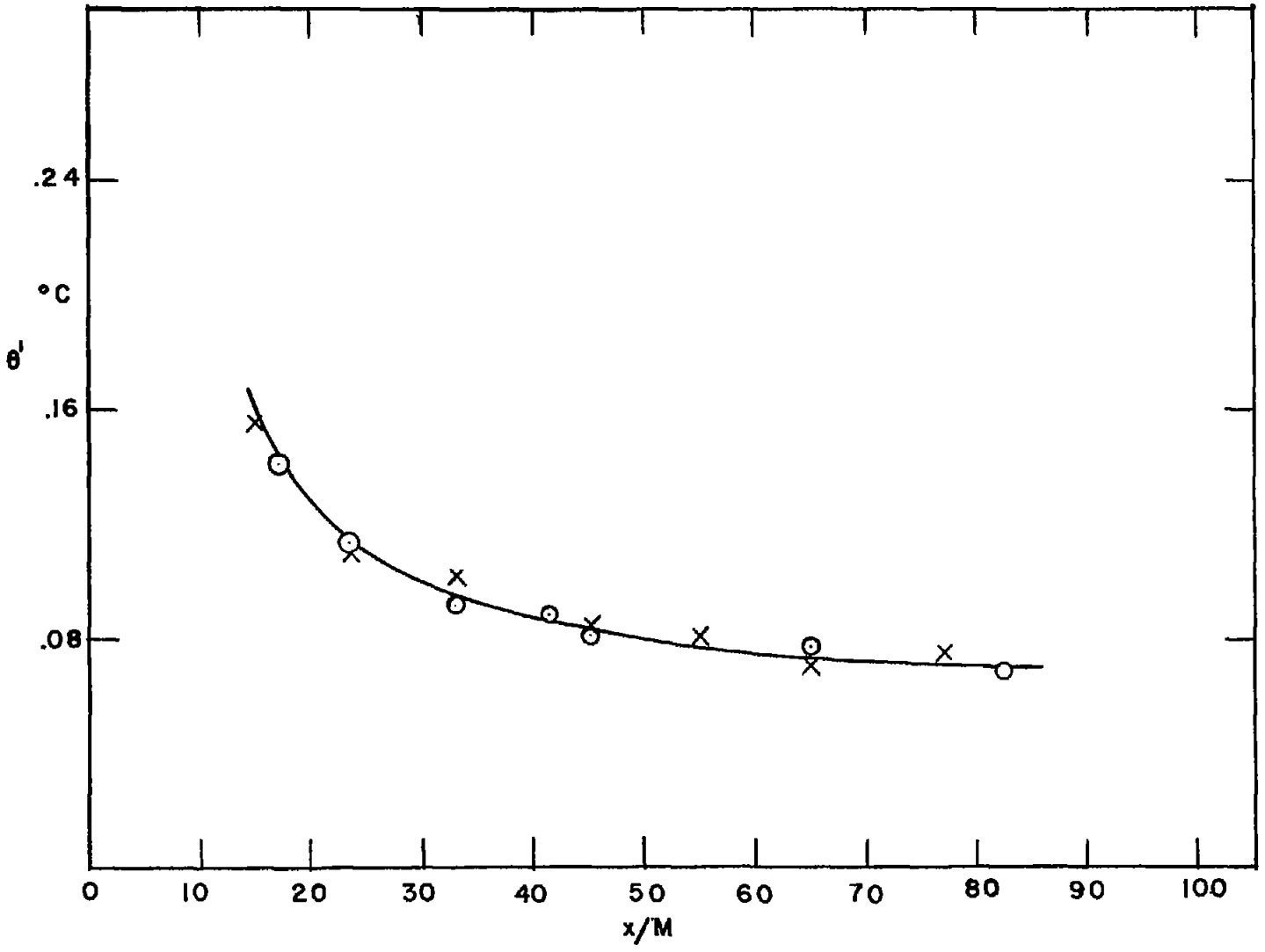

Figure 11. - Temperature fluctuation decay.

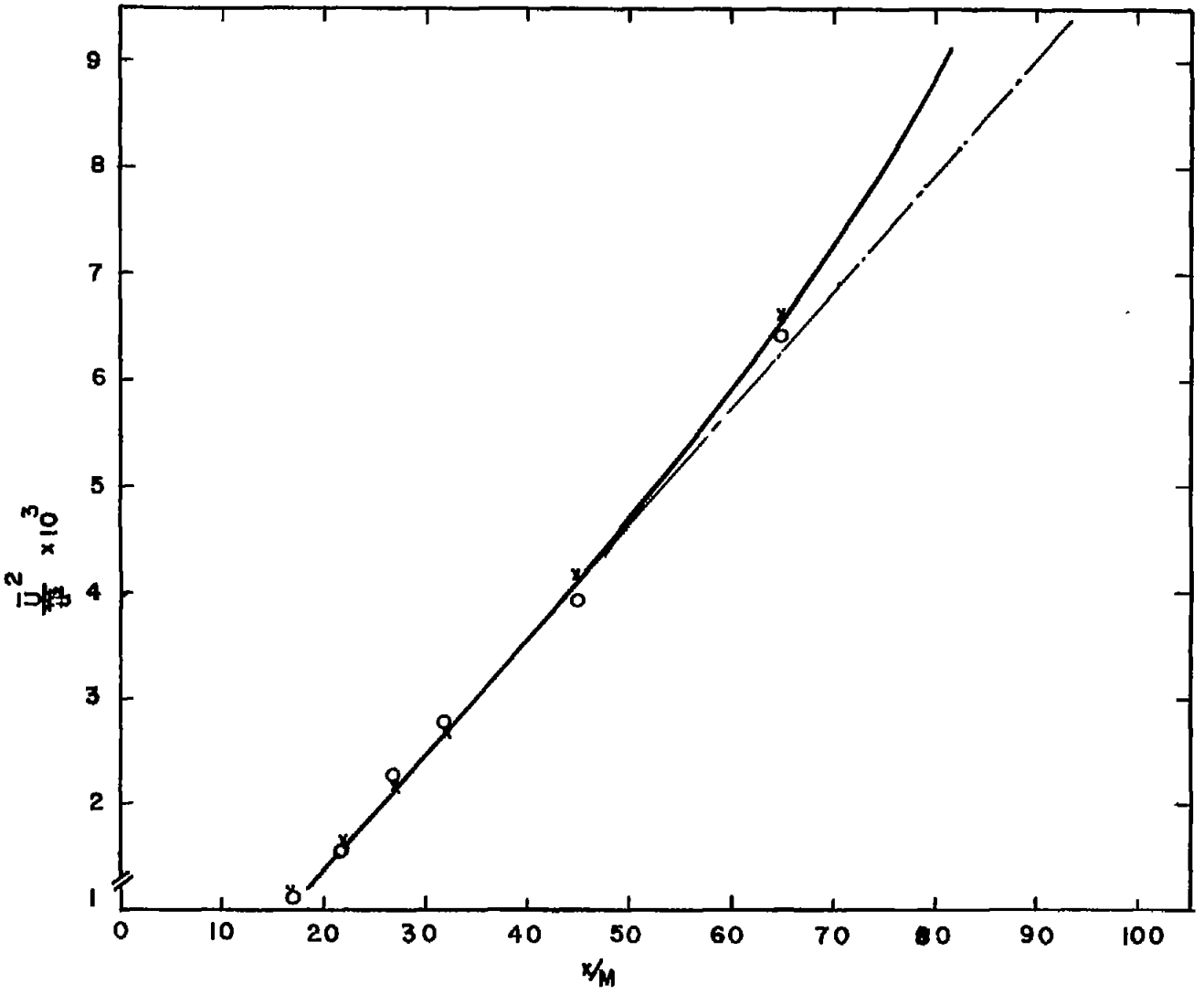

Figure 12. - Inverse squares of longitudinal turbulence decay (fig. 10).

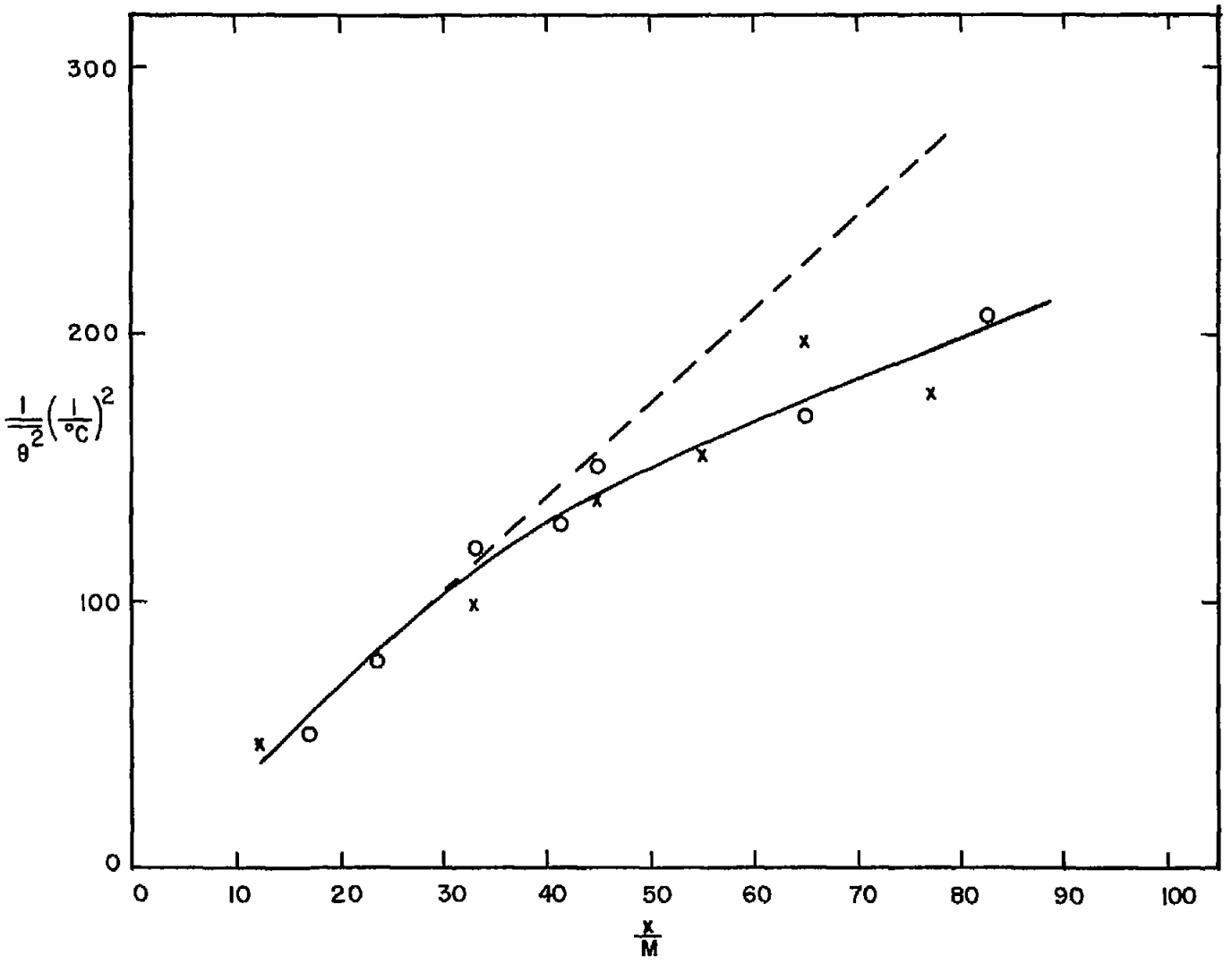

Figure 13. - Inverse squares of temperature fluctuation decay (fig. 11).

4934 CP-6 back

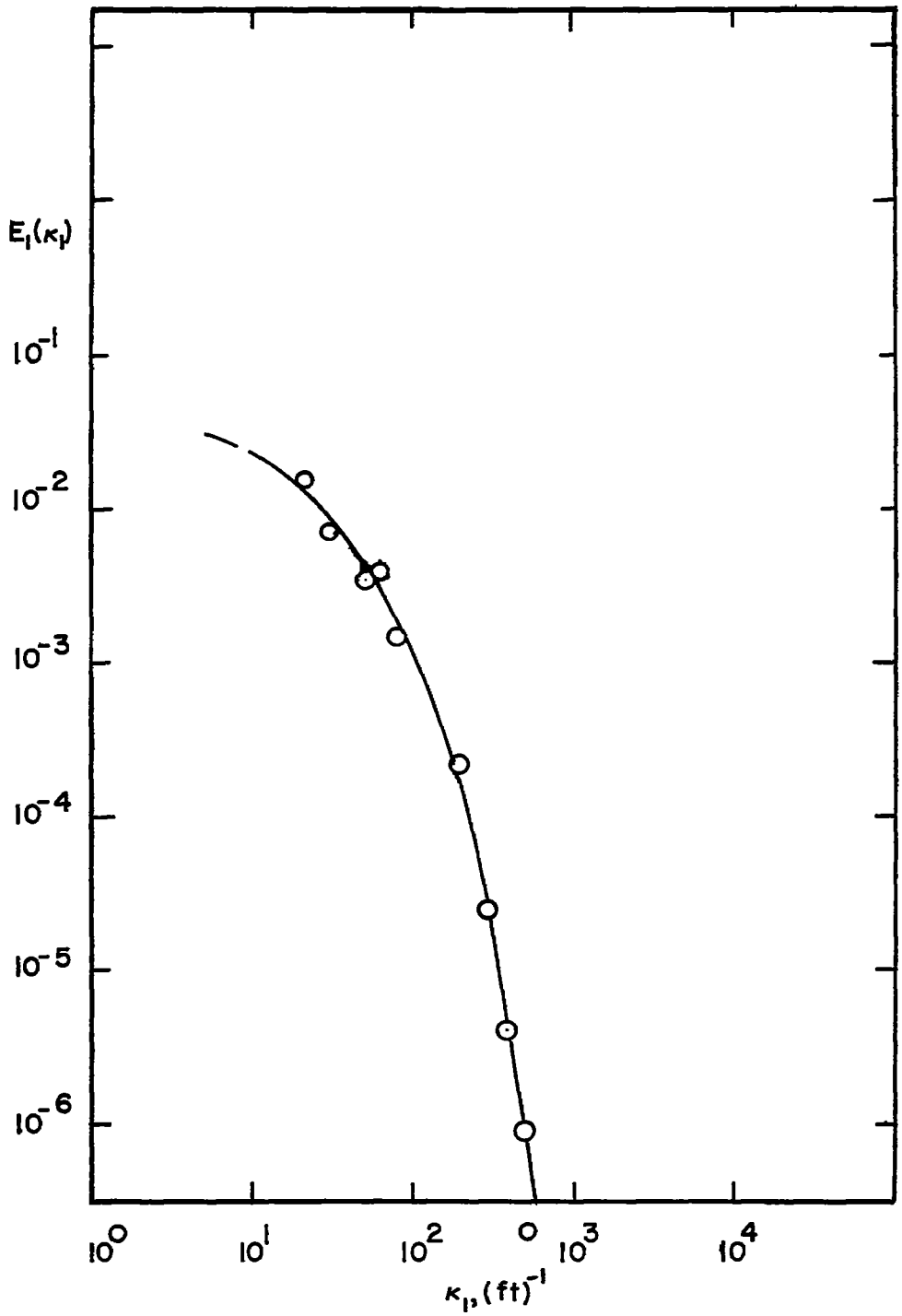

(a) $\overline{u^2}$.

Figure 14. - Time spectra of $\overline{u^2}$ and $\overline{\theta^2}$. x/M = 17.0.

4934

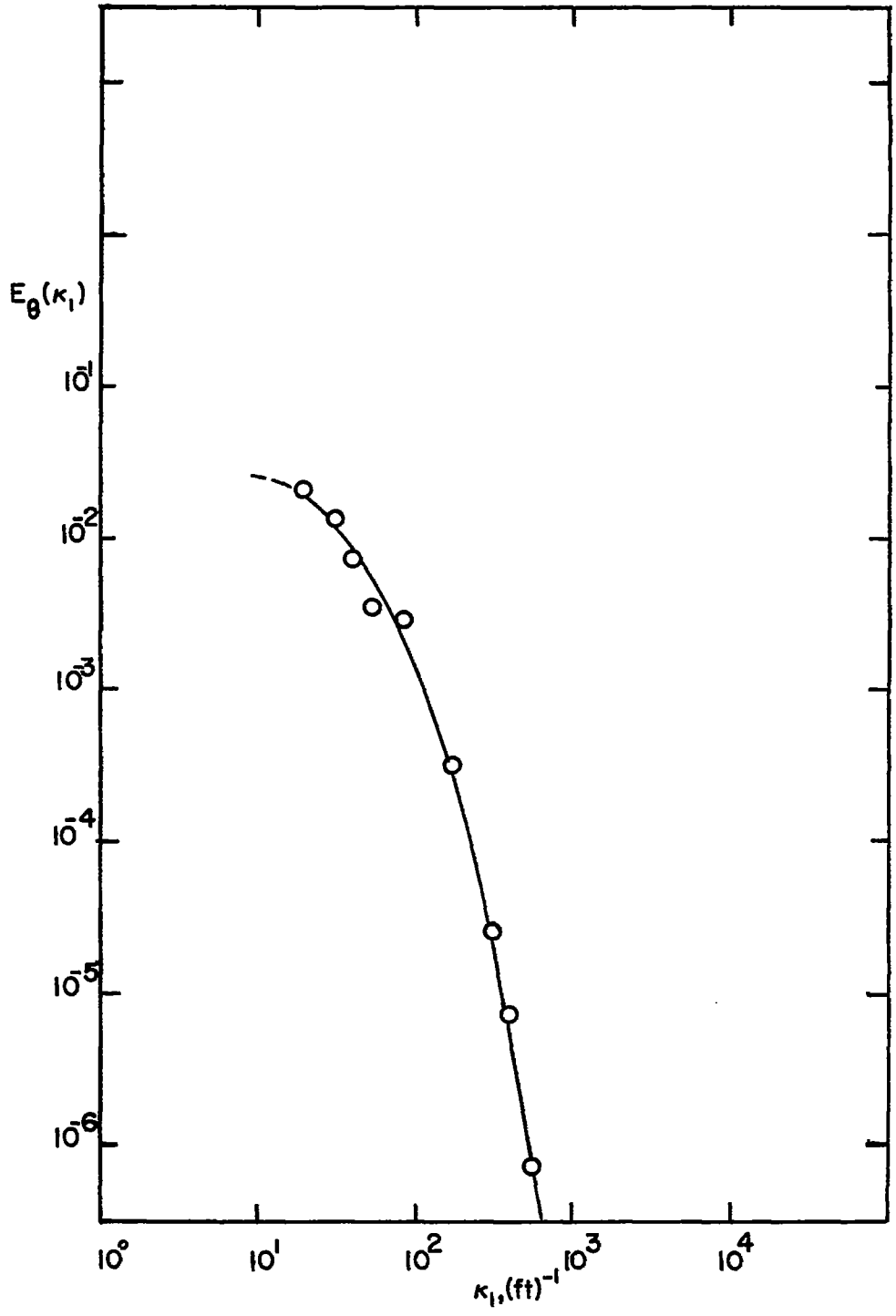

(b) $\overline{\theta^2}$.

Figure 14. - Concluded. Time spectra of $\overline{u^2}$ and $\overline{\theta^2}$. x/M = 17.0.

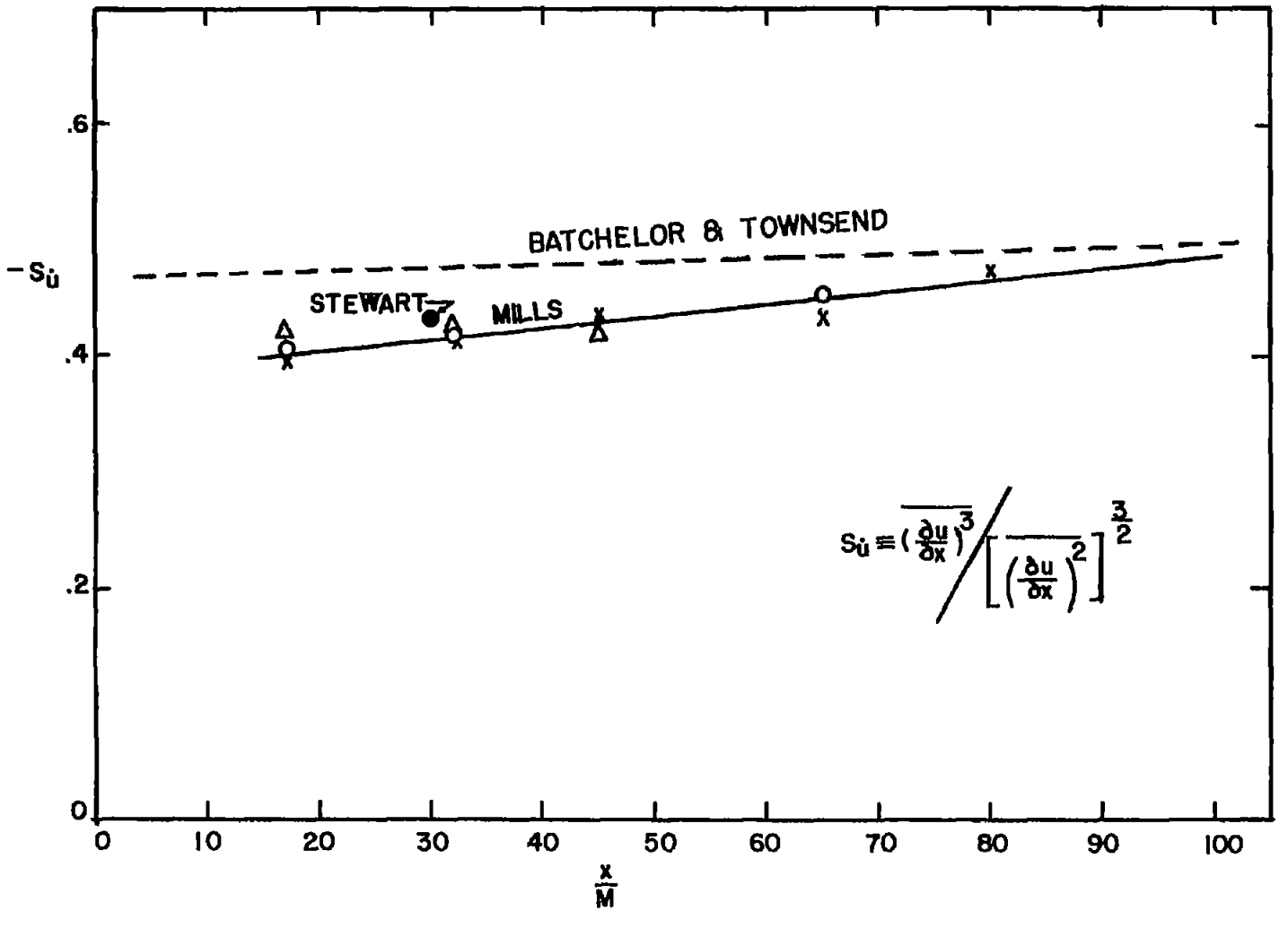

Figure 15. - Skewness of velocity derivatiye $S_{\dot{u}}$ as function of x/M.

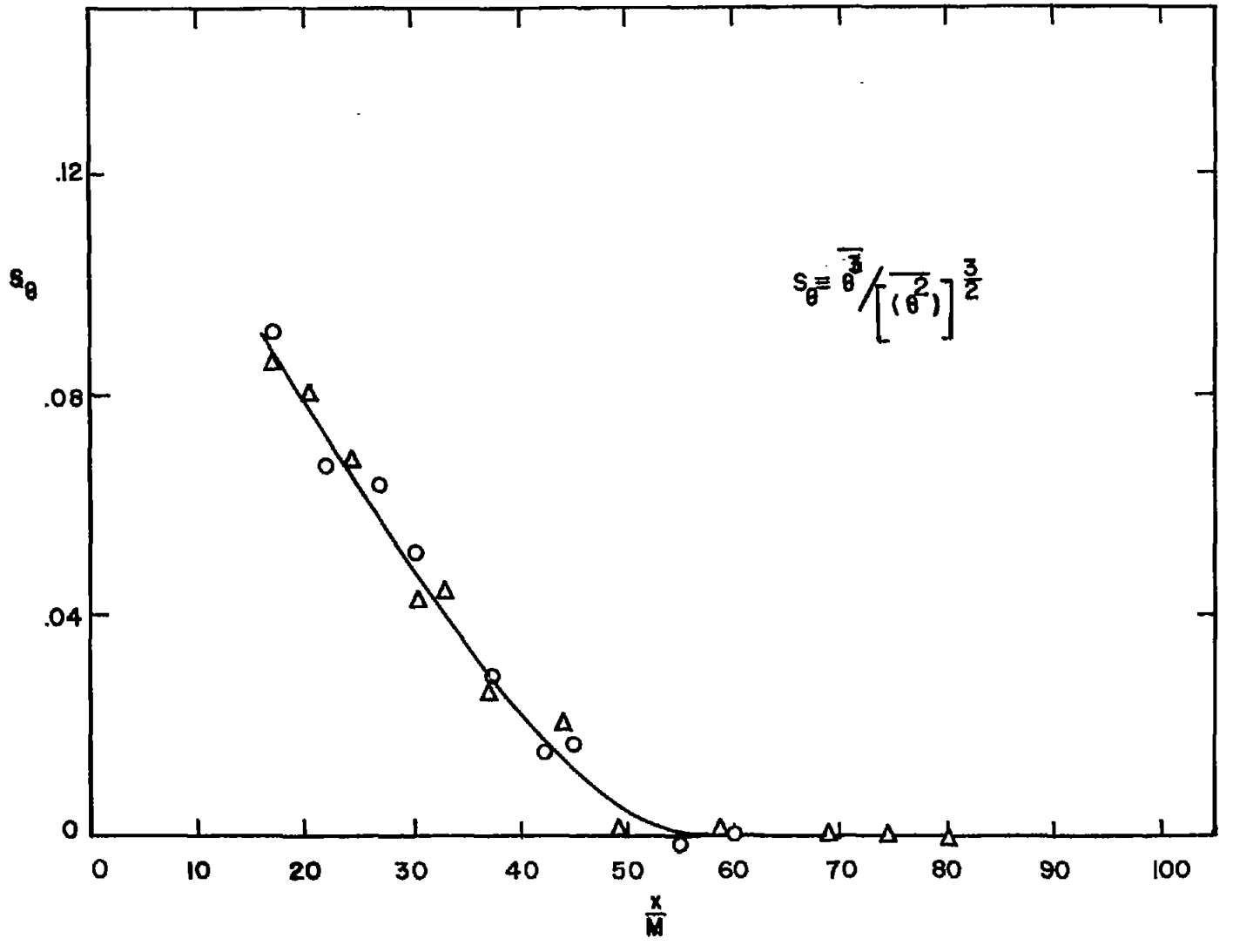

Figure 16. - Skewness of temperature fluctuation S_θ as function of x/M.

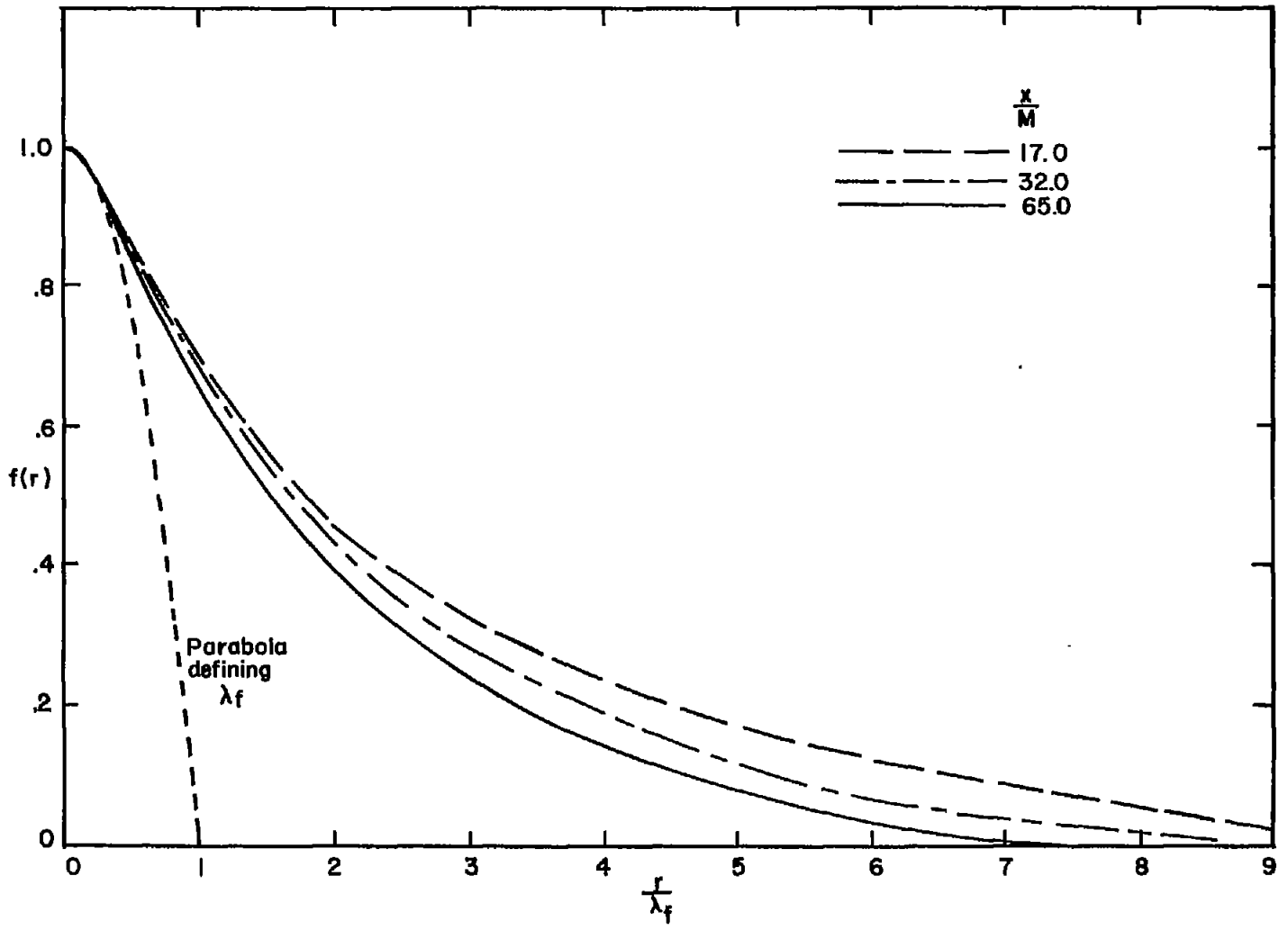

(a) Faired data.

Figure 17. - Longitudinal velocity correlations for various x/M.

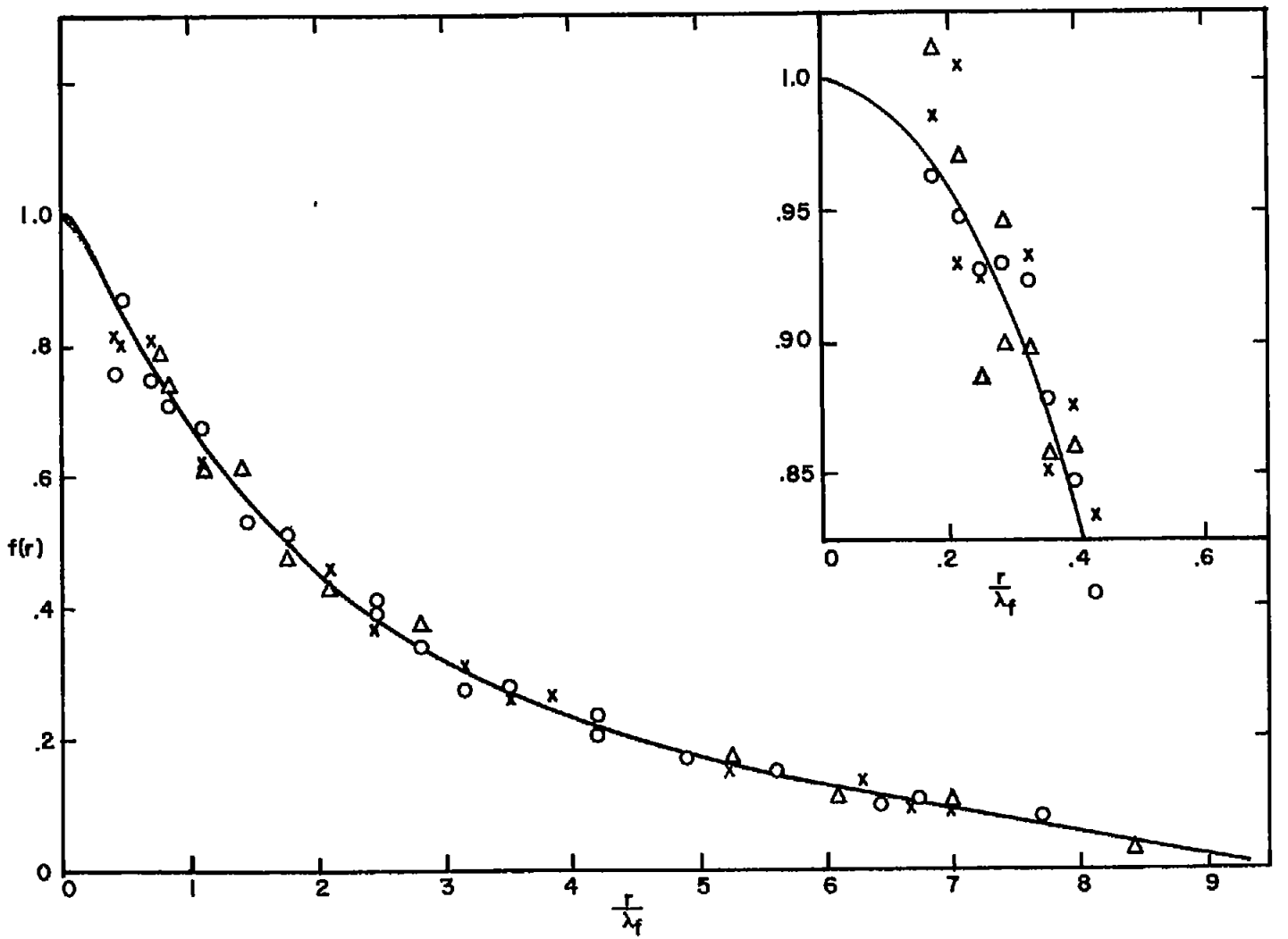

(b) Actual measured values at x/M = 17.0.

Figure 17. - Concluded. Longitudinal velocity correlations for various x/M.

4934 CP-7

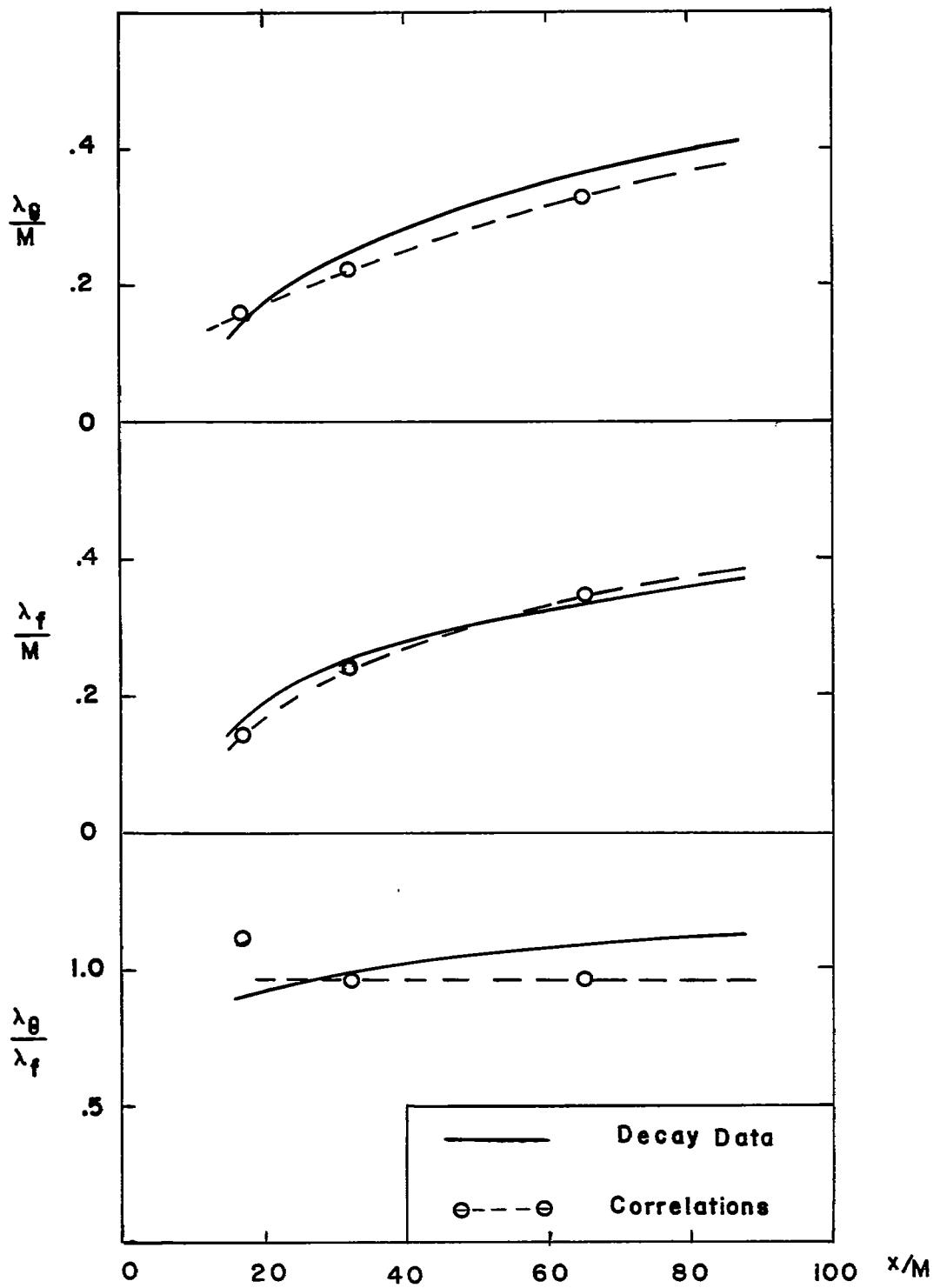

Figure 18. - Variation of temperature and longitudinal velocity fluctuation microscales with x/M.

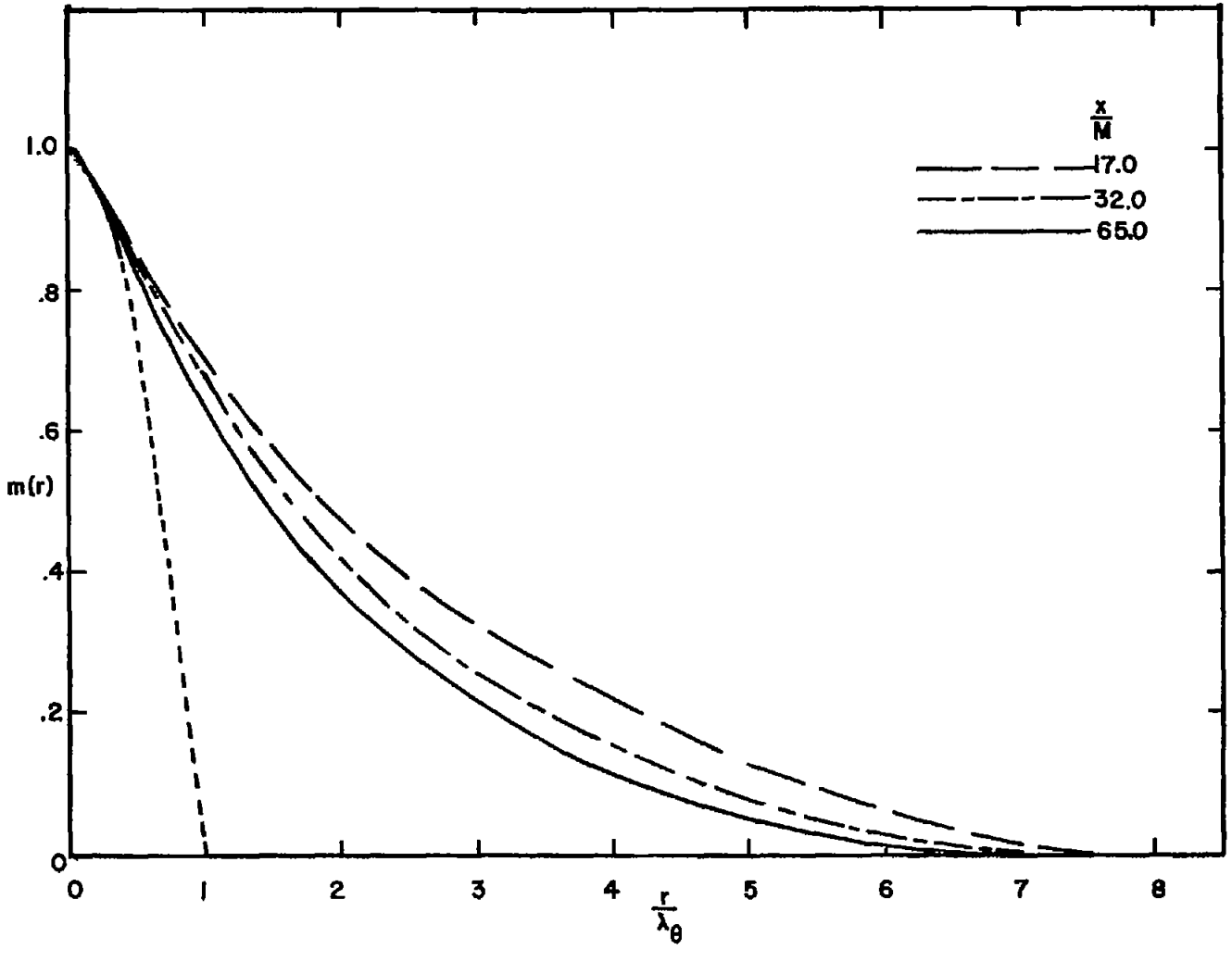

(a) Faired data.

Figure 19. - Temperature double correlations for various x/M.

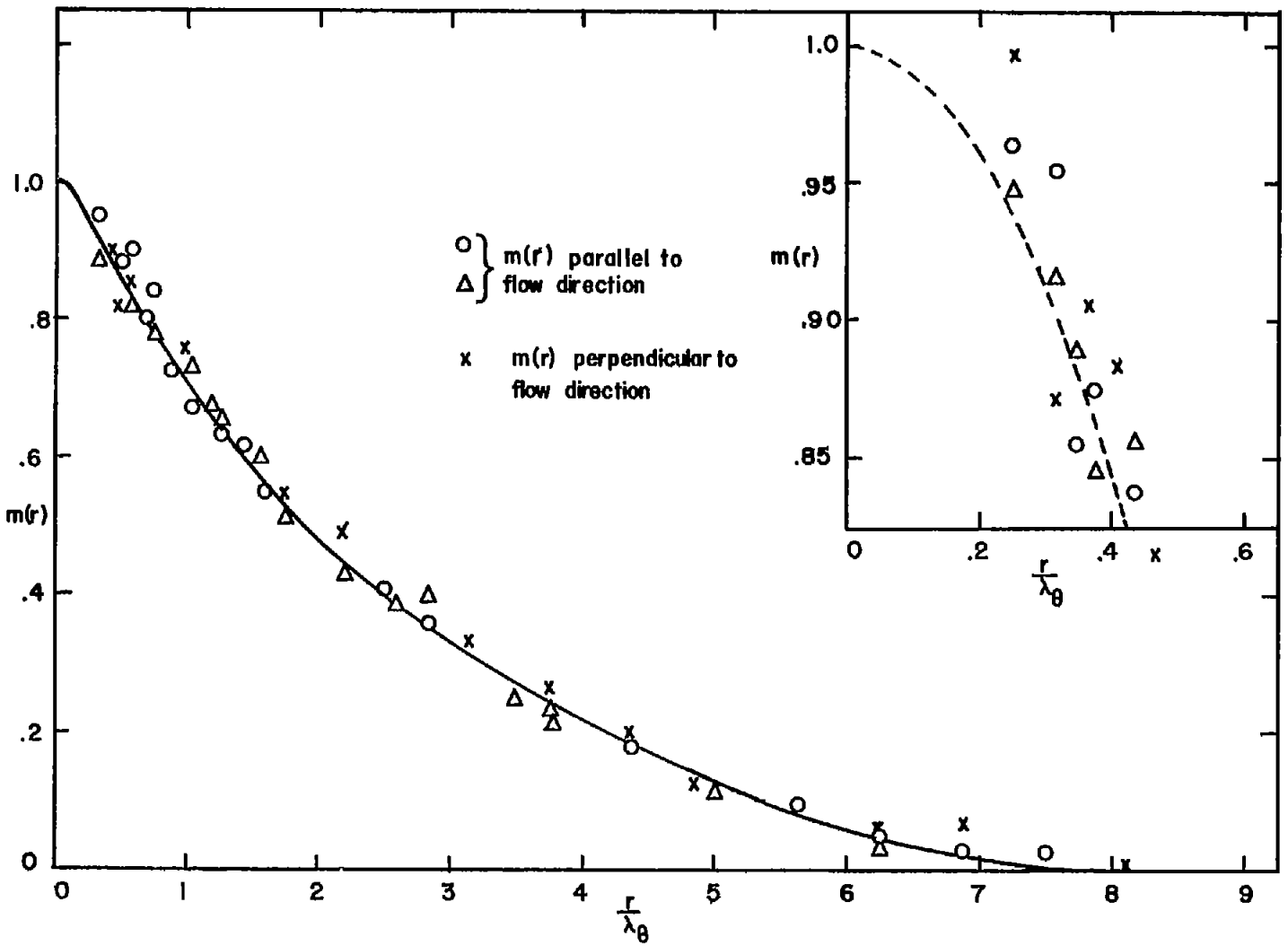

(b) Actual data measured at x/M = 17.0.

Figure 19. - Concluded. Temperature double correlations for various x/M.

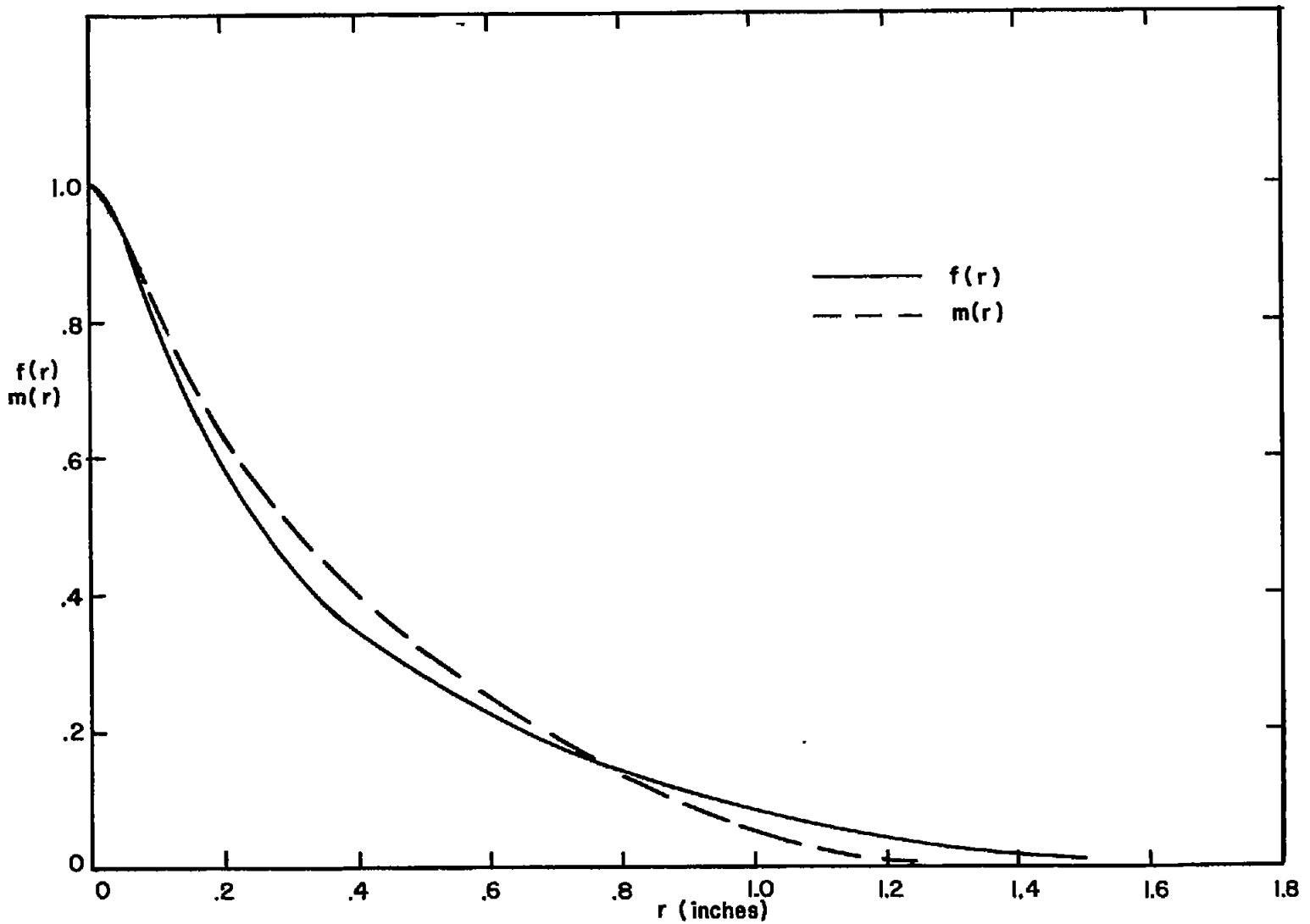

Figure 20. - Contrast between f(r) and m(r). x/M = 17.0.

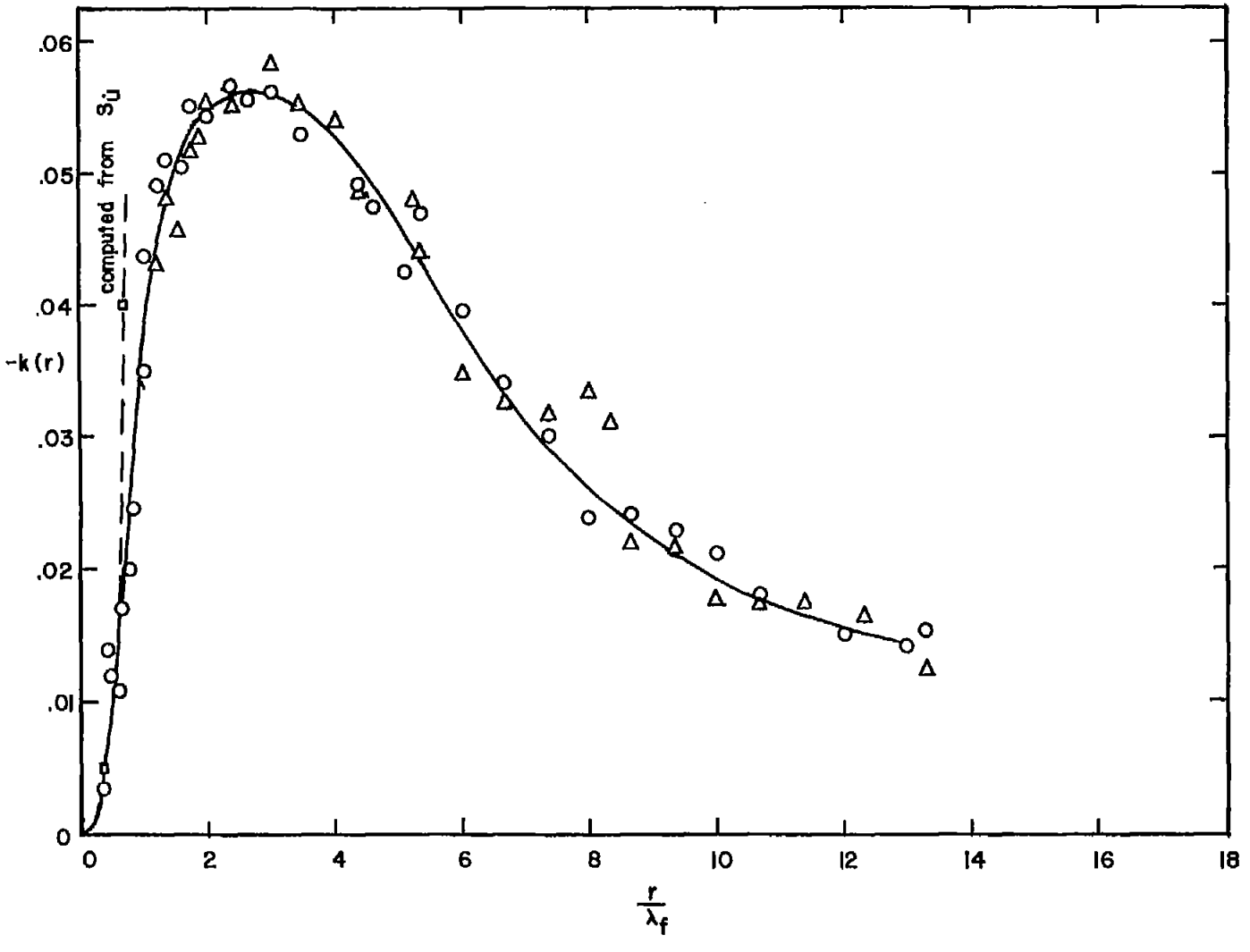

(a) x/M = 17.0.

Figure 21. - Triple velocity correlations for various x/M.

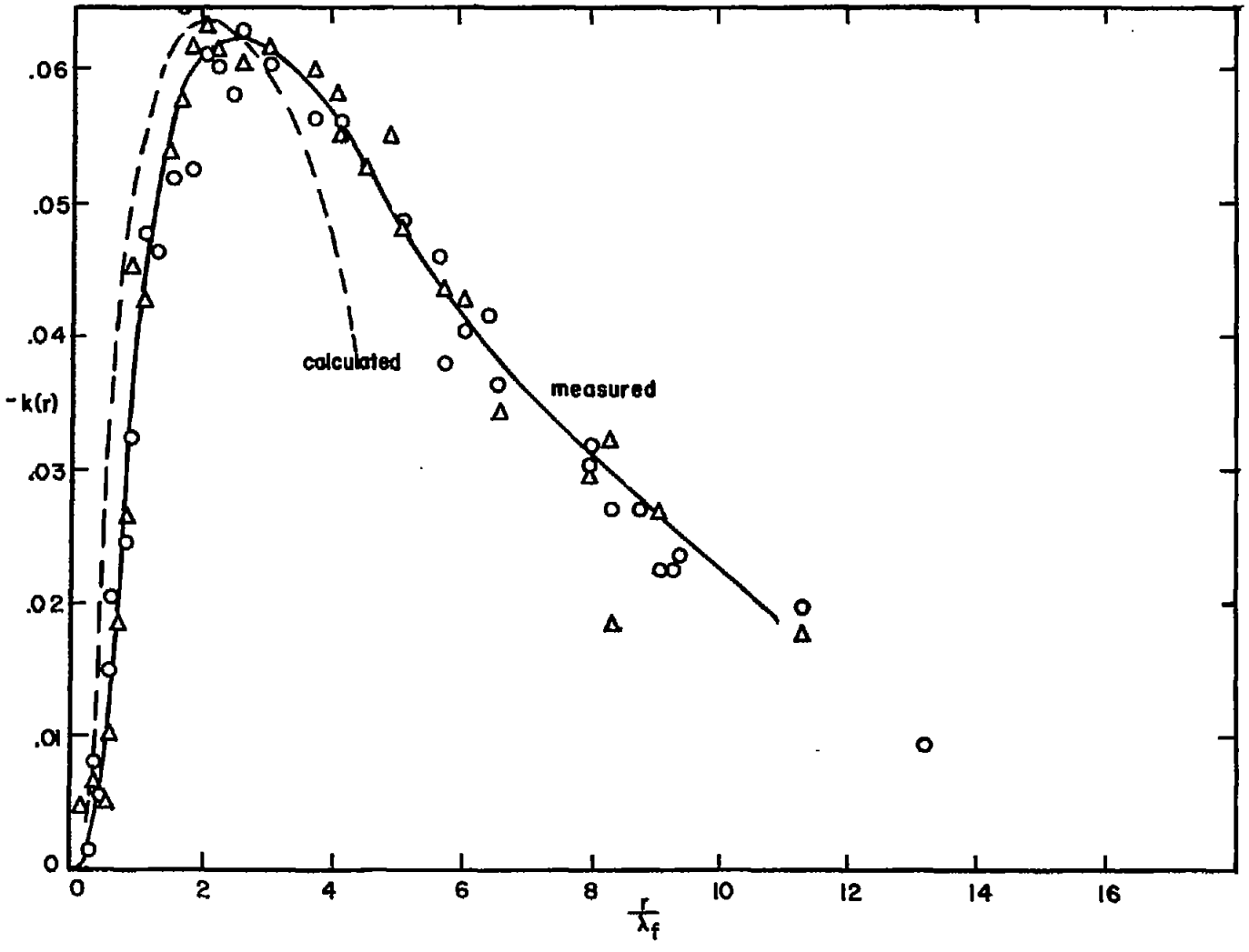

(b) x/M = 32.0.

Figure 21. - Continued. Triple velocity correlations for various x/M.

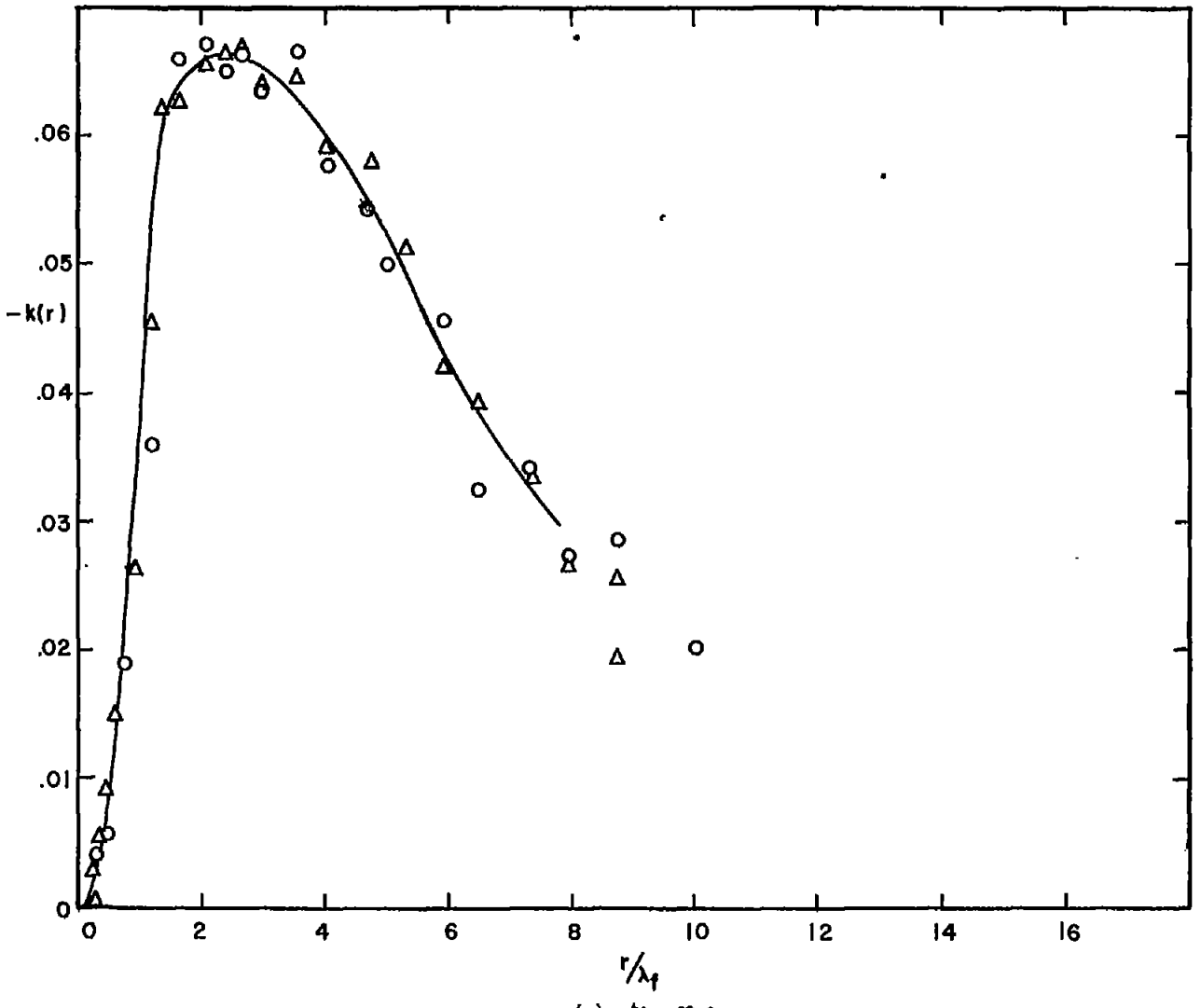

(c) x/M = 69.0.

Figure 21. - Concluded. Triple velocity correlations for various x/M.

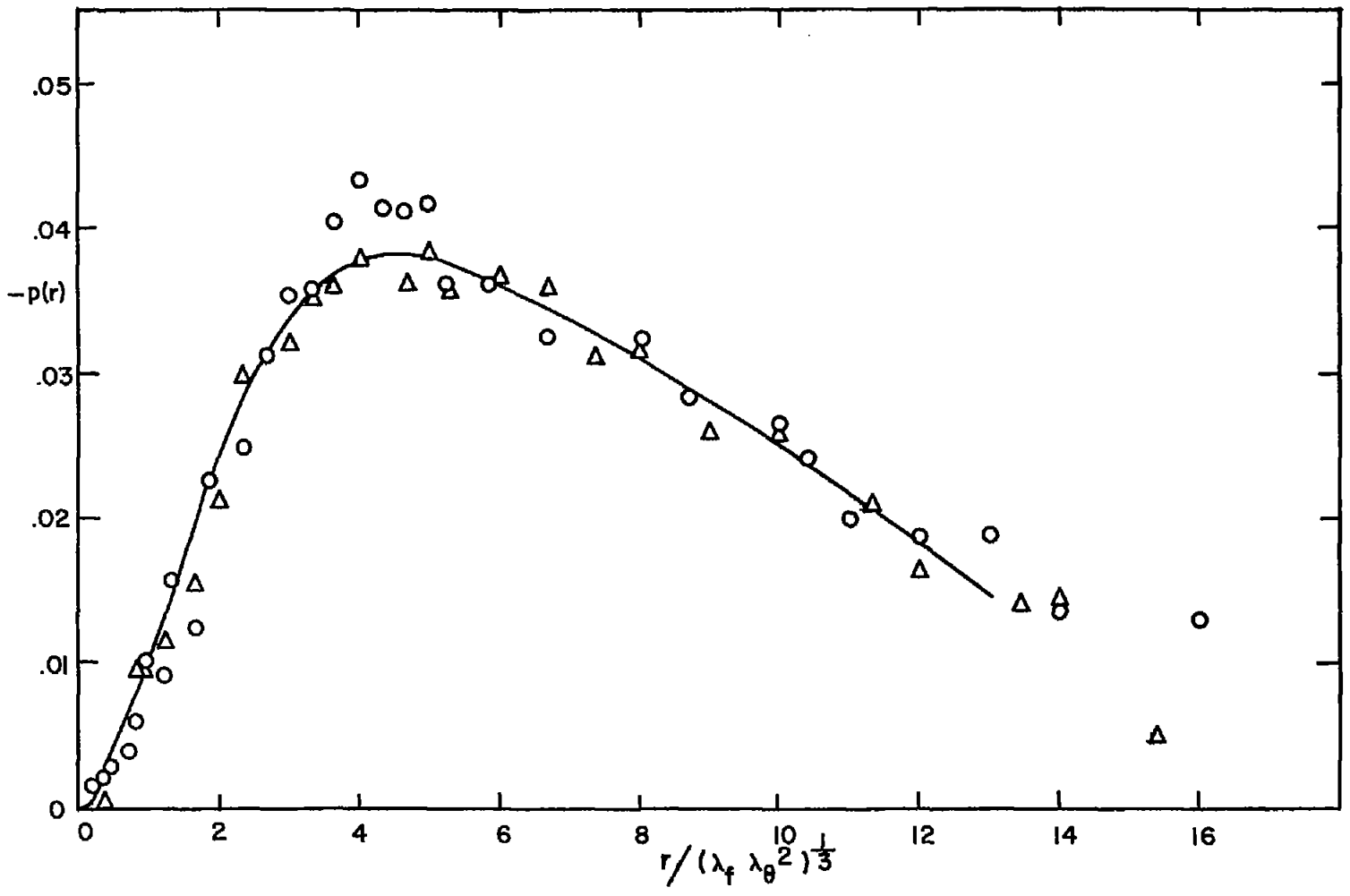

(a) x/M = 17.0.

Figure 22. - Mixed temperature-velocity correlation coefficient.

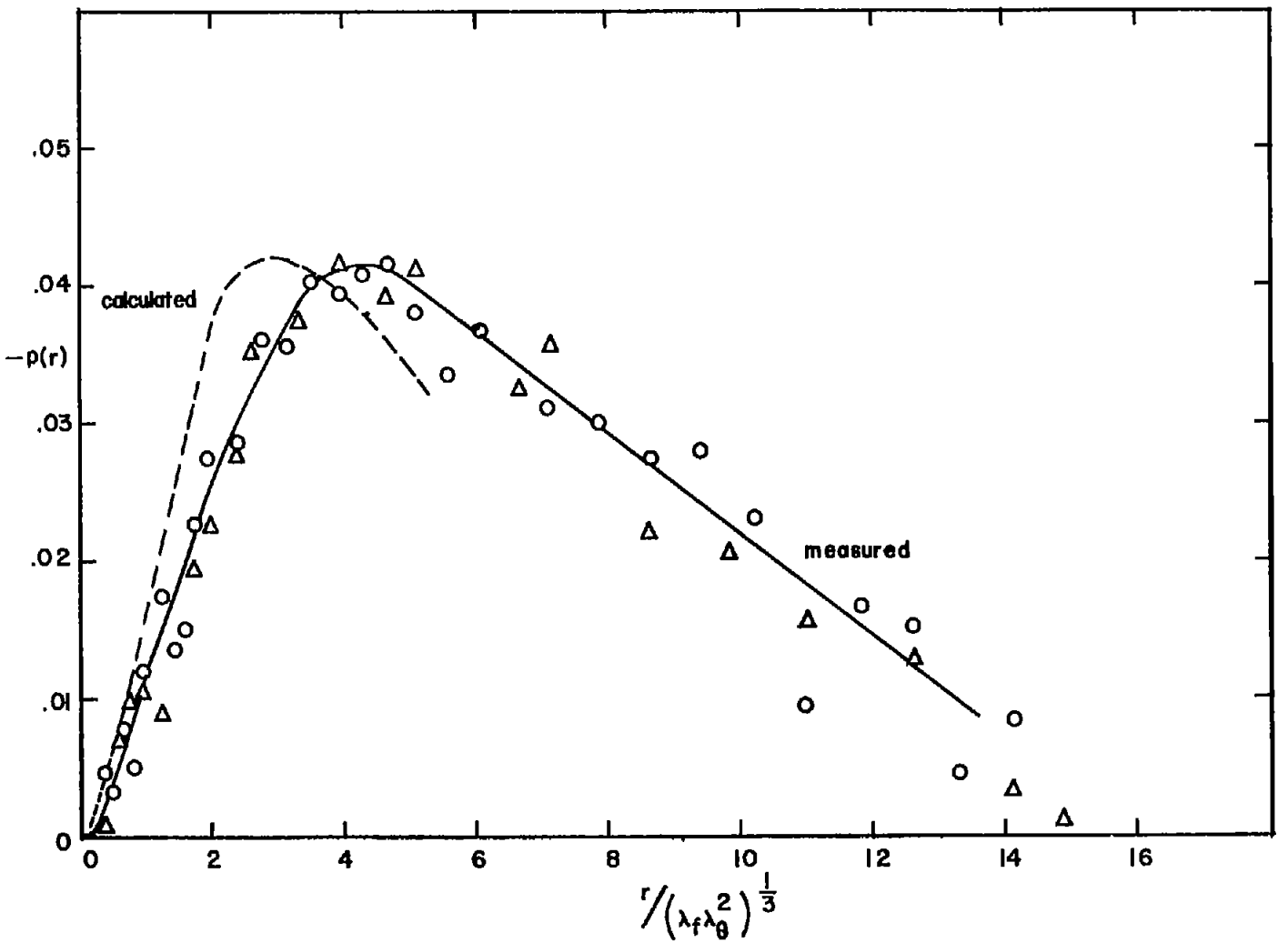

(b) x/M = 32.0.

Figure 22. - Continued. Mixed temperature-velocity correlation coefficient.

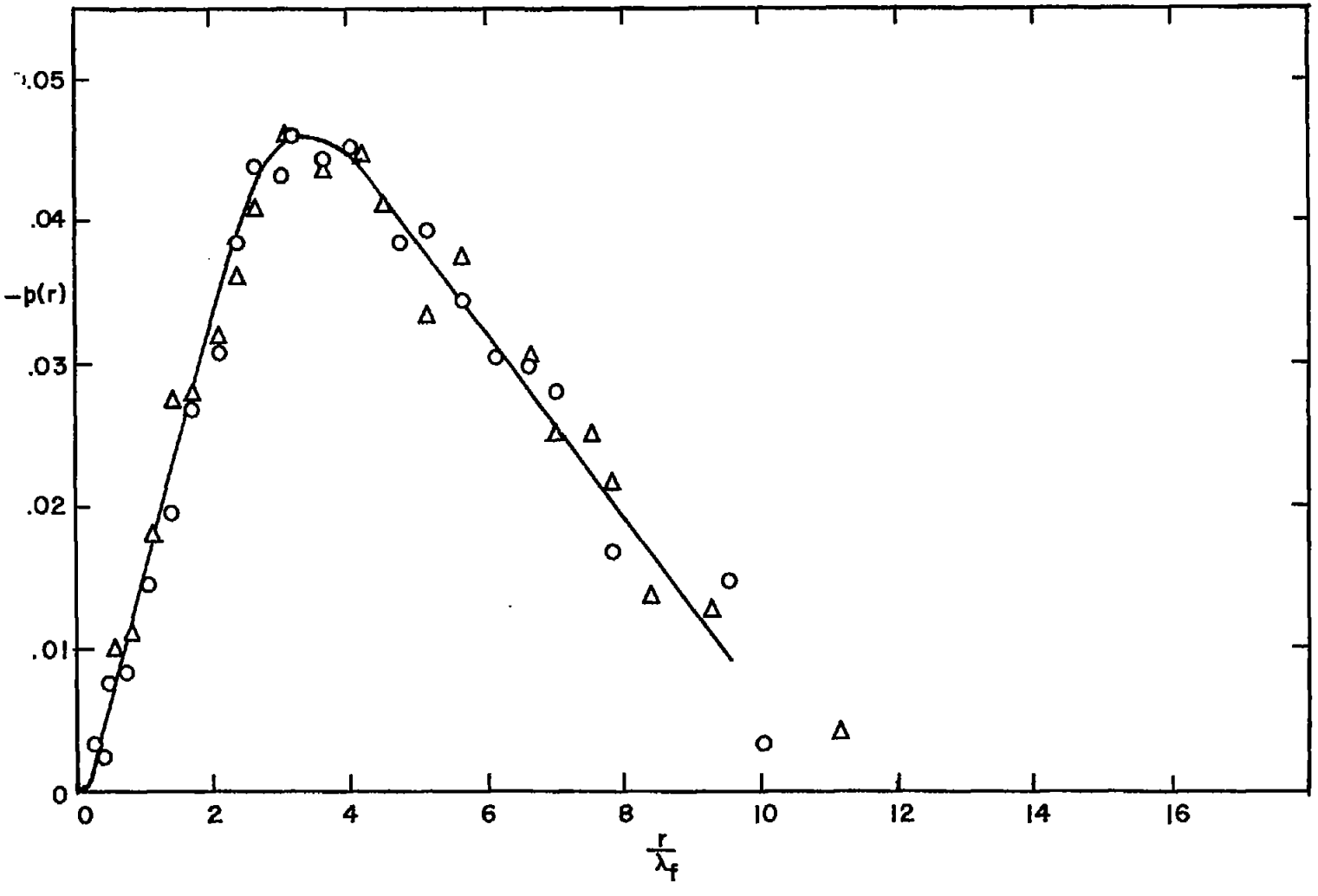

(c) x/M = 69.0.

Figure 22. - Concluded. Mixed temperature-velocity correlation coefficient.

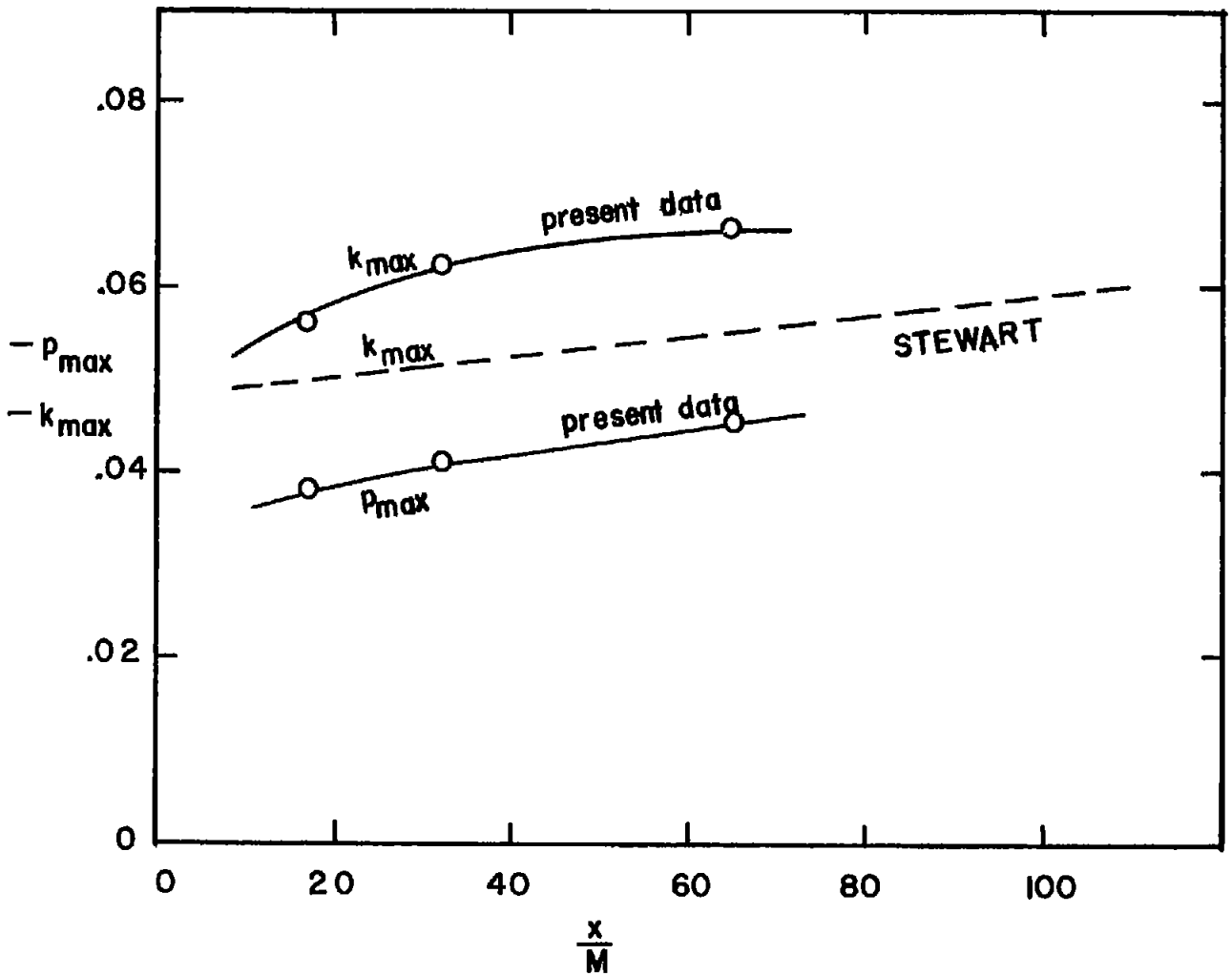

Figure 23. - Variation of maximum values of k and p with x/M.

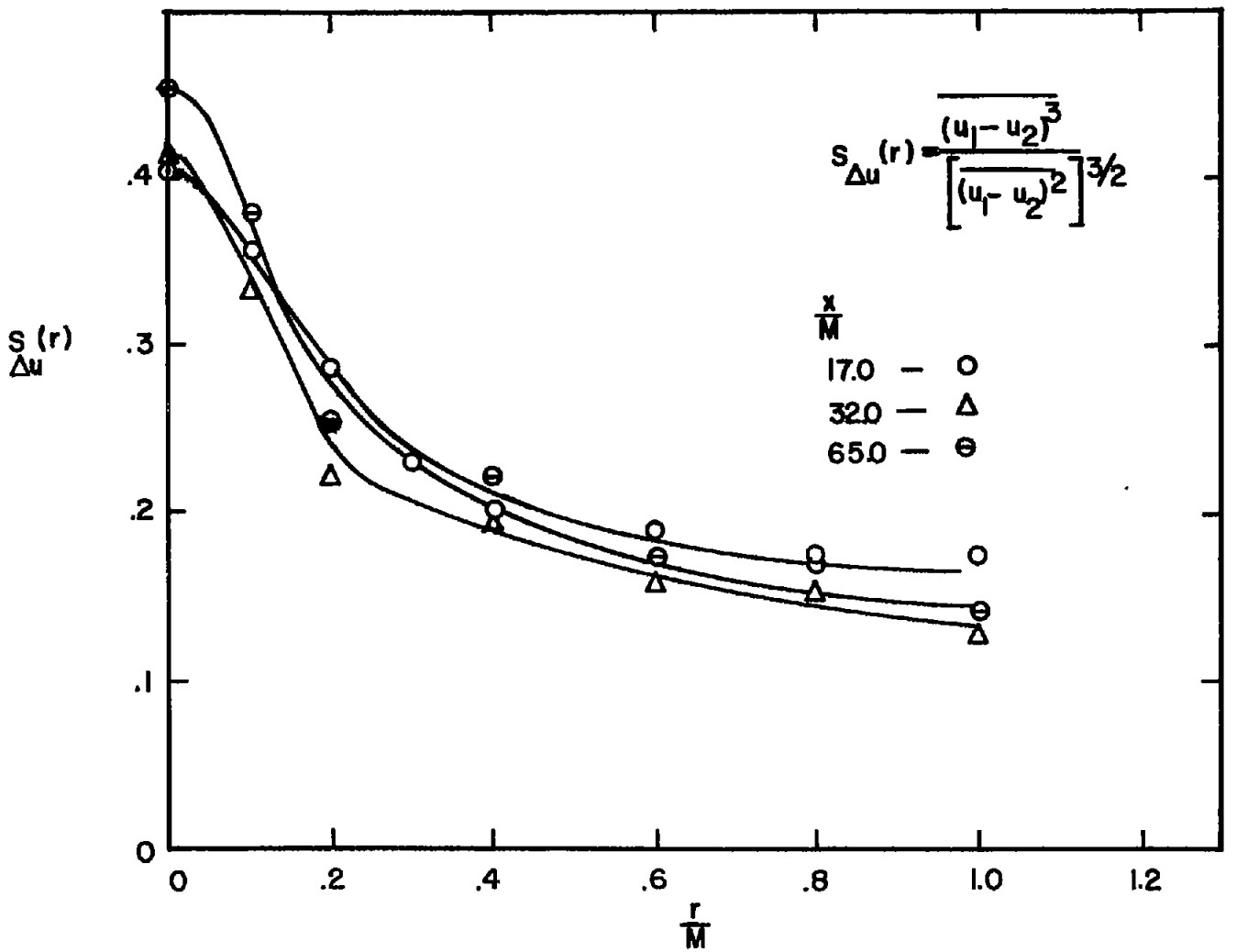

Figure 24. - Function $S_{\Delta u}(r)$ at various x/M.

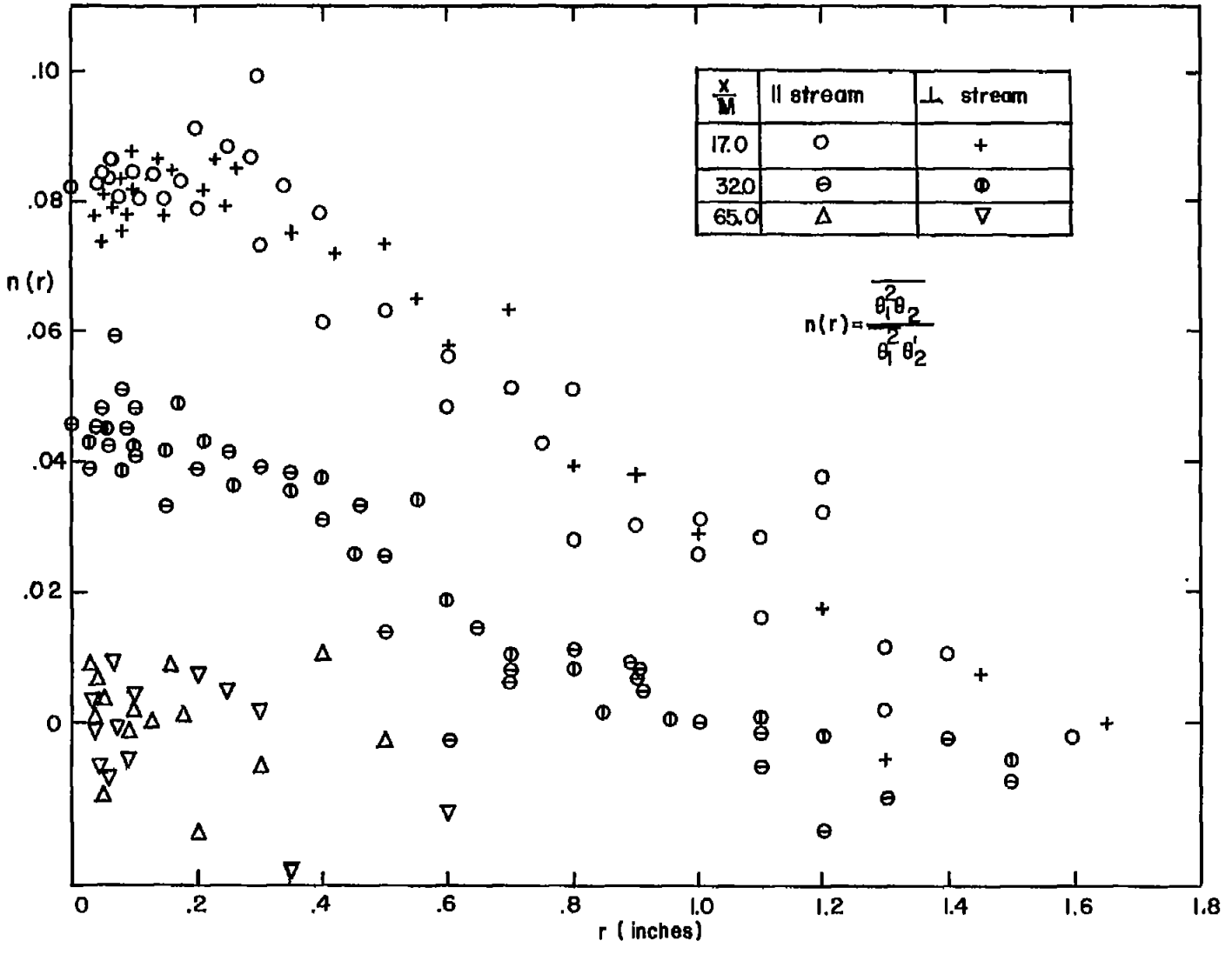

Figure 25. - Triple temperature correlation n(r) as function of r.

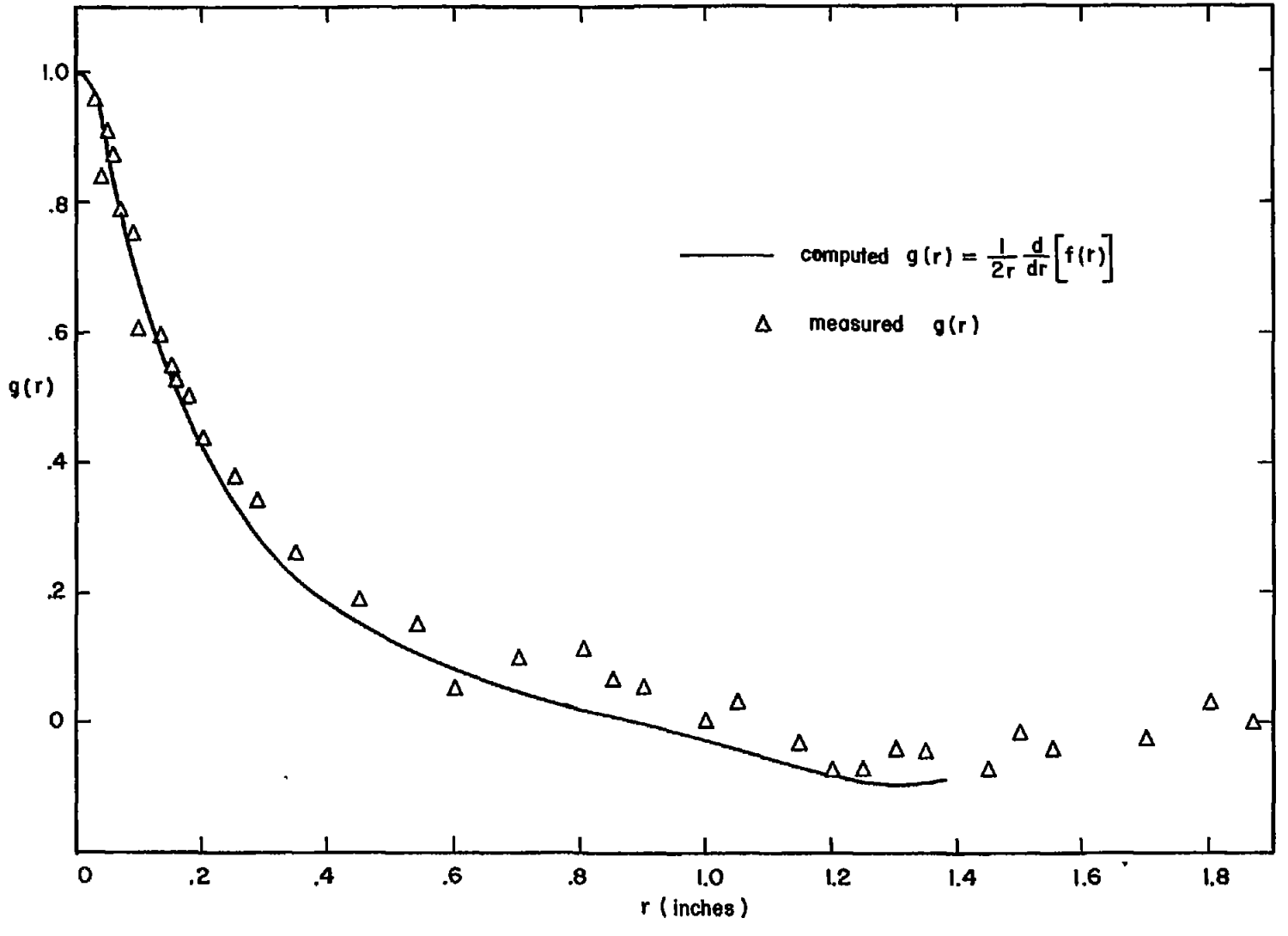

Figure 26. - Measured values of g(r). x/M = 17.0.

4934

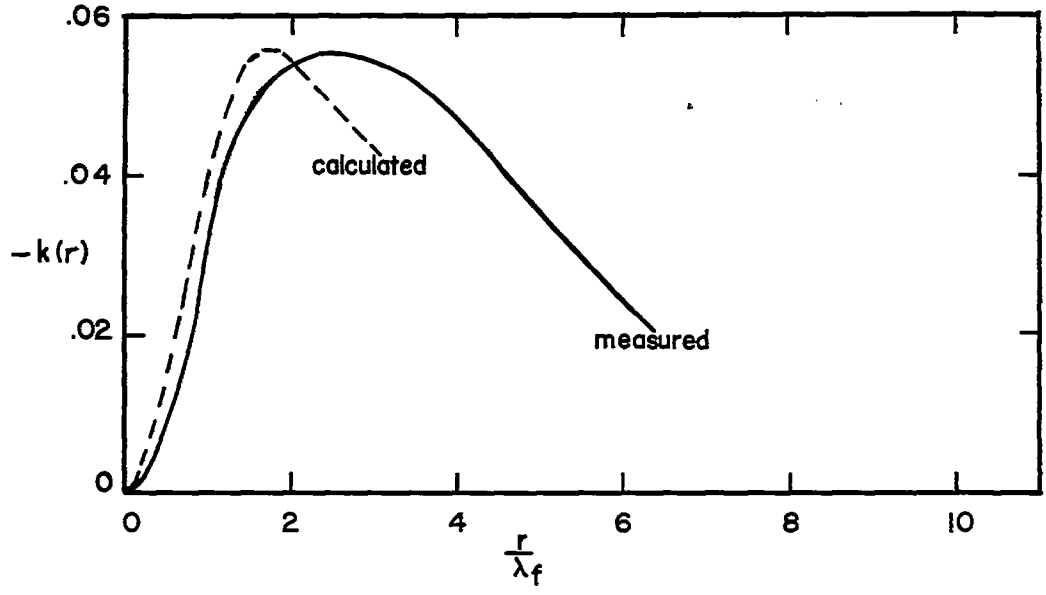

(a) Data of reference 12. x/M = 60.0.

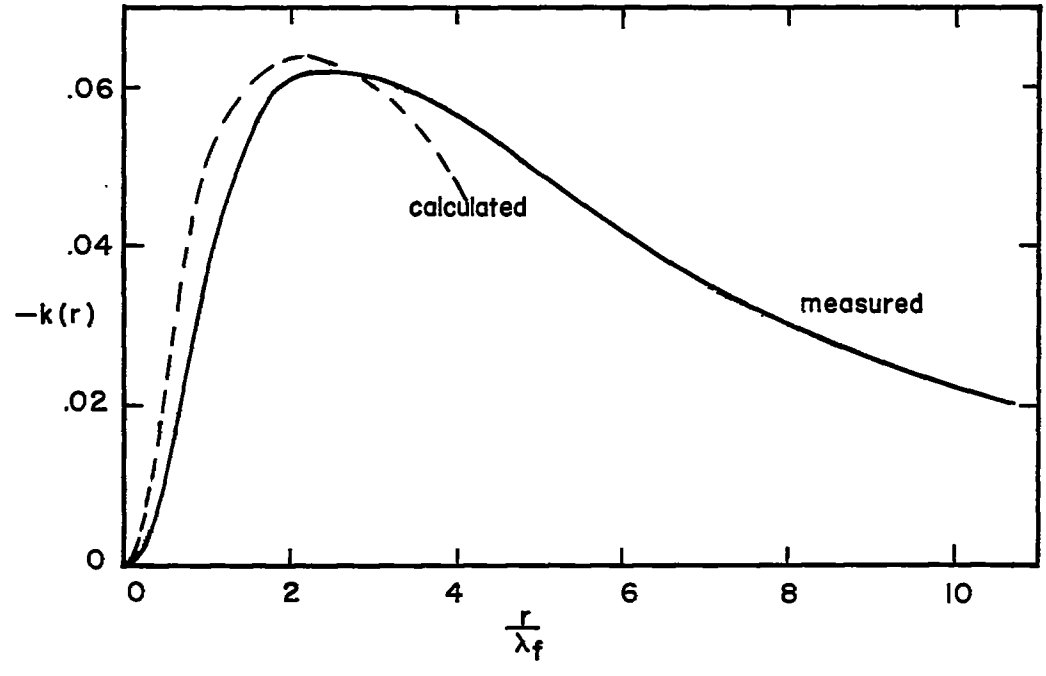

(b) Present data. x/M = 32.0.

Figure 27. - Comparison of measured values of triple correlation with values predicted from equation (14).

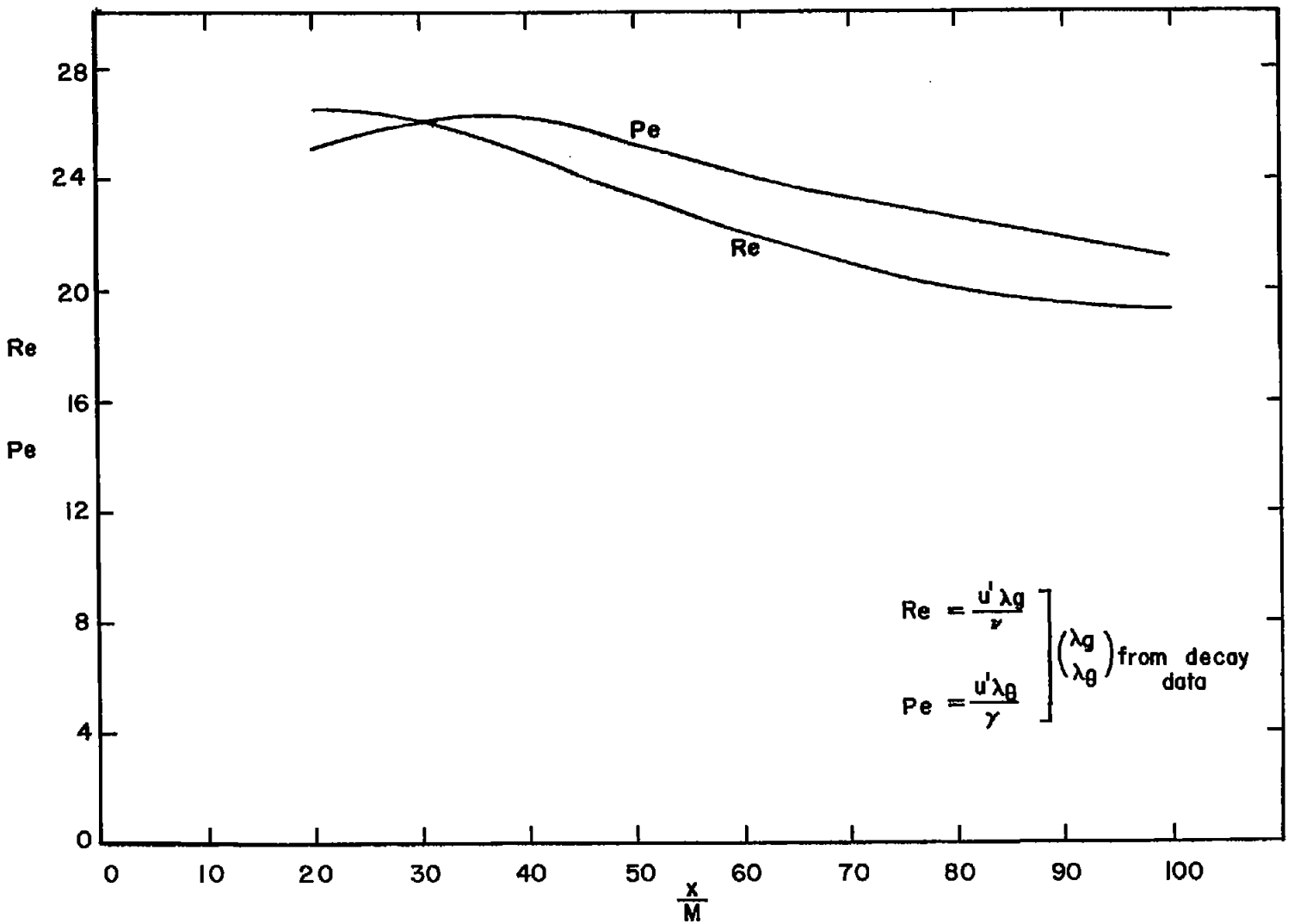

Figure 28. - Variation in Reynolds and Peclet numbers.

4934

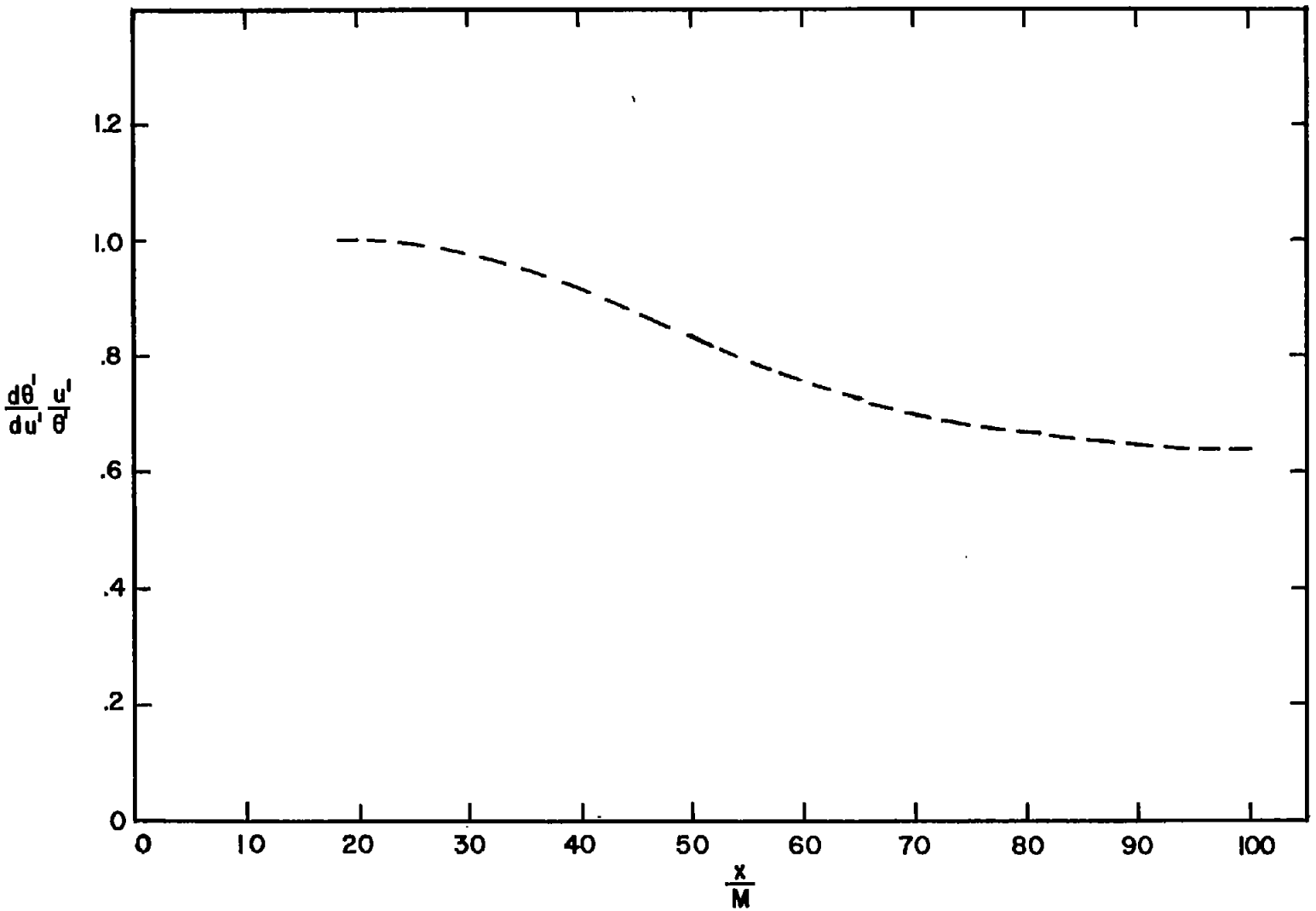

Figure 29. - Relative decay rates of temperature and velocity fluctuations.

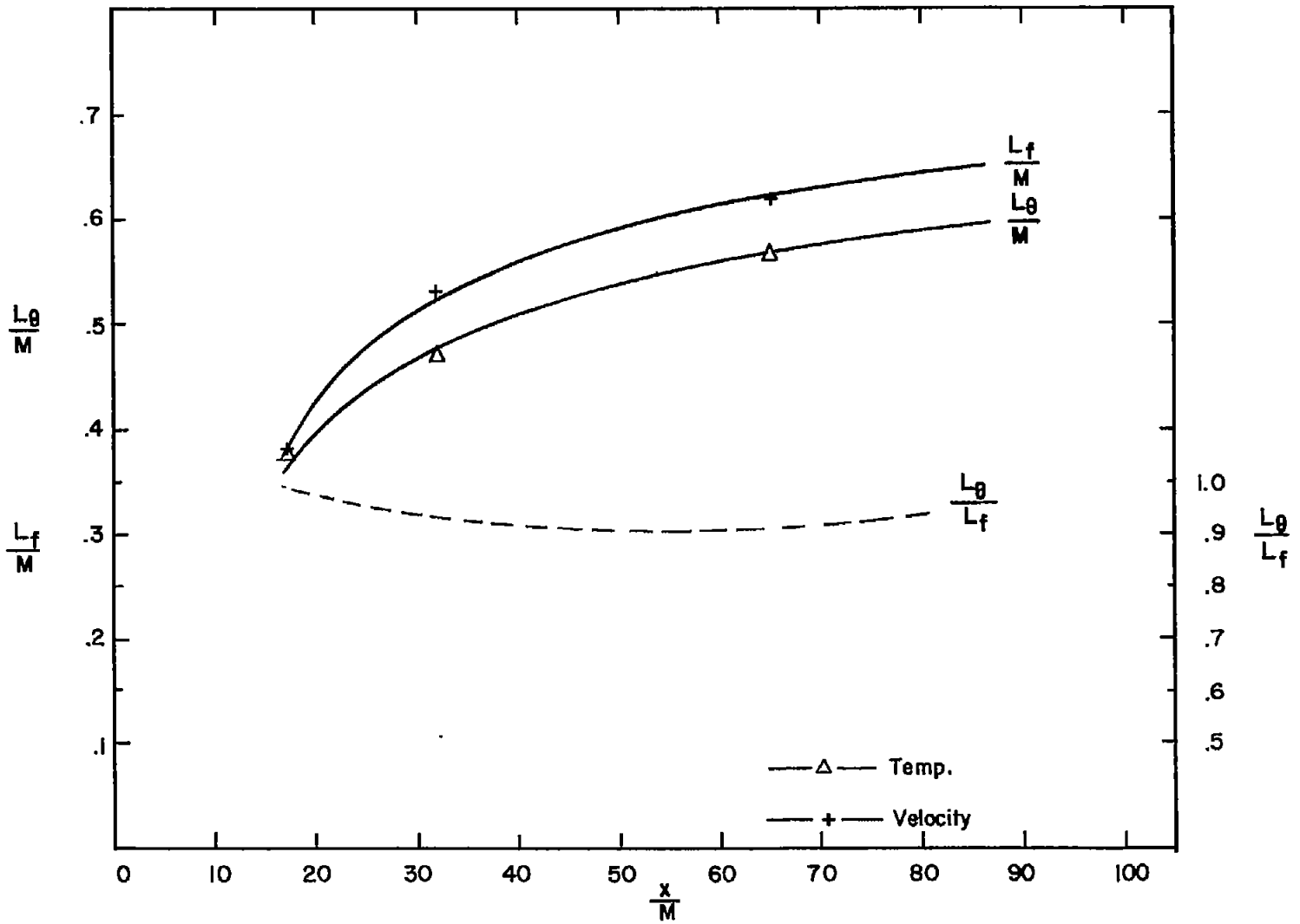

Figure 30. - Integral scales.

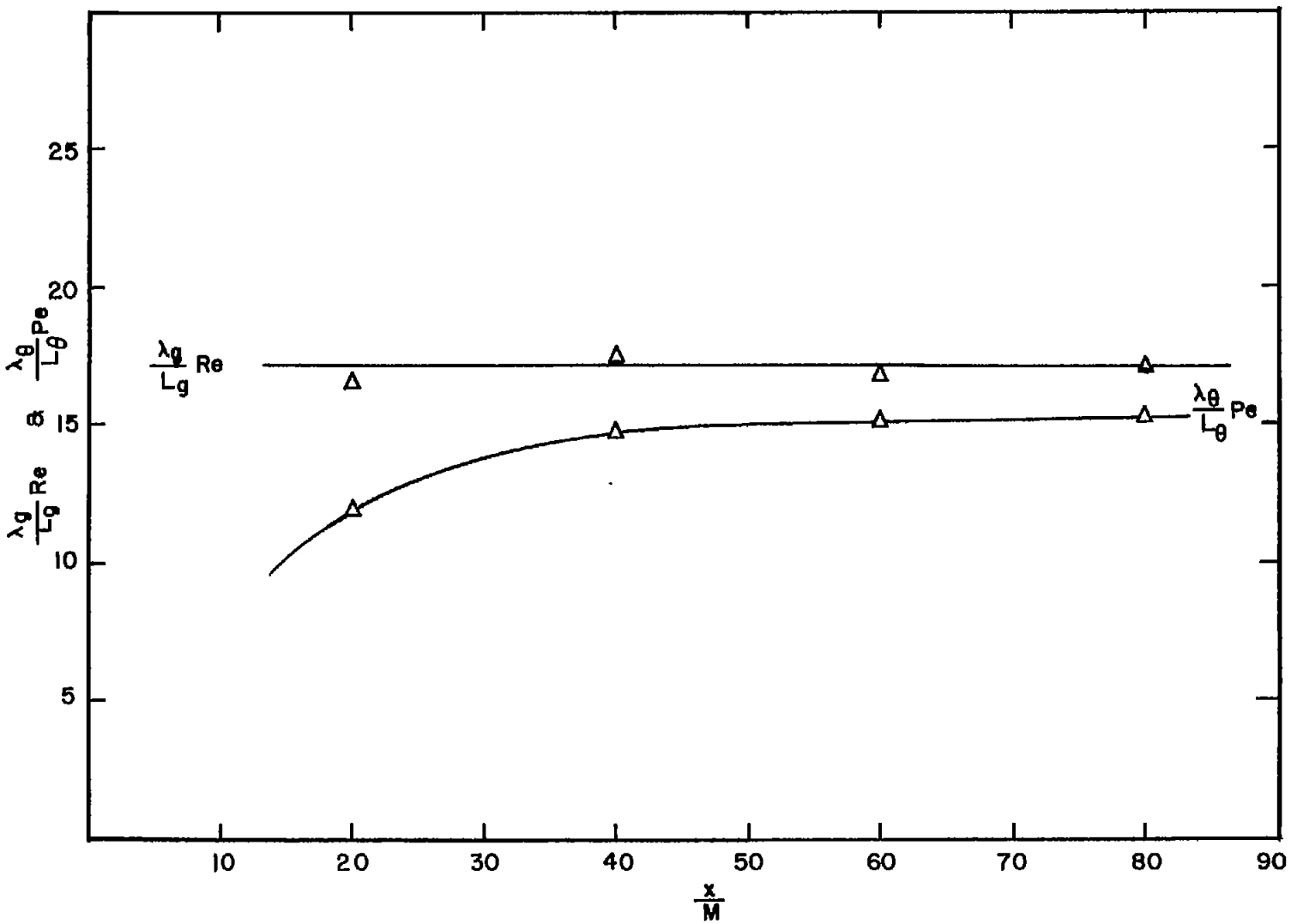

Figure 31. - Demonstration of the approach to similarity of temperature and velocity fields at large values of x/M.